Conf-9111204--1

WSRC-RP-91-1001

UNDERWATER VAPOR PHASE BURNING OF ALUMINUM PARTICLES AND ON ALUMINUM IGNITION DURING STEAM EXPLOSIONS (U)

DOES NOT CONTAIN
UNCLASSIFIED CONTROLLED
NUCLEAR INFORMATION

Reviewing Official: Philip G Ellison
Philip G. Ellison

Date: octobr 7th, 1991

Westinghouse Savannah River Company
Savannah River Site
Aiken, SC 29808

PREPARED FOR THE US DEPARTMENT OF ENERGY UNDER CONTRACT NO. DE-AC09-89SR18035

DISCLAIMER

WSRC-RP--91-1001

DE92 011196

SA&RM
SEVERE ACCIDENT PROGRAM

UNDERWATER VAPOR PHASE BURNING OF ALUMINUM PARTICLES AND ON ALUMINUM IGNITION DURING STEAM EXPLOSIONS (U)

by

Michael Epstein

Fauske & Associates
Burr Ridge, Illinois

Reviewed by

P.G. Ellison & M.L. Hyder
Westinghouse Savannah River Company
Aiken, South Carolina

and

Hans K. Fauske
President
Fauske & Associates

September 1991

Westinghouse Savannah River Company
Savannah River Site
Aiken, SC 29808

PREPARED FOR THE US DEPARTMENT OF ENERGY UNDER CONTRACT NO. DE-AC09-89SR18035

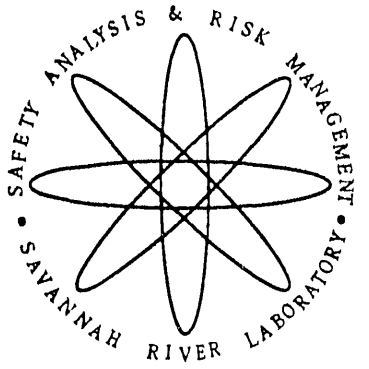

PROJECT: Steam Explosions of Aluminum Alloys

DOCUMENT: WSRC-RP-91-1001

TITLE: UNDERWATER VAPOR PHASE BURNING OF ALUMINUM PARTICLES AND ON ALUMINUM IGNITION DURING STEAM EXPLOSIONS (U)

TASK: Severe Accident Program Documentation

APPROVALS

Phillip G. Ellison
Derivative Classifier — Date: Oct 7th, 1991

Phillip G. Ellison
Technical Review — Date: Oct 7th, 1991

M.L. Hyder
Technical Review — Date: Oct 7, 1991

L.A. Wooten, Manager
Safety Analysis Group — Date: Oct 8, 1991

M.J. Hitchler, Manager
Reactor Safety Research — Date: 10/9/91

UNDERWATER VAPOR PHASE BURNING OF ALUMINUM PARTICLES AND ON ALUMINUM IGNITION DURING STEAM EXPLOSIONS

Submitted To:

Westinghouse Savannah River Company
Aiken, South Carolina

Prepared By:

Fauske & Associates, Inc.
16W070 West 83rd Street
Burr Ridge, Illinois 60521
(708) 323-8750

PREPARED BY: Michael Epstein

Michael Epstein
Vice President

REVIEWED BY: _____

Hans K. Fauske
President

TABLE OF CONTENTS

TABLE OF CONTENTS (Continued)

LIST OF FIGURES

LIST OF FIGURES (Continued)

LIST OF TABLES

ABSTRACT

Recently reported experimental studies on aluminum-water steam explosions indicate that there may be a critical metal temperature at which the process changes over from a physical explosion to one which is very violent and involves the rapid liberation of chemical energy. In this report we examine the hypothesis that vapor-phase burning of aluminum is a necessary condition for the occurrence of such "ignition-type" steam explosions. An available two-phase stagnation flow film-boiling model is used to calculate the steam flux to the vaporizing aluminum surface. Combining this calculation with the notion that there is an upper limit to the magnitude of the metal vaporization rate at which the reaction regime must change from vapor phase to surface burning, leads to prediction of the critical metal surface temperature below which vapor phase burning is impossible. The critical temperature is predicted for both the aluminum-water pre-mixture configuration in which coarse drops of aluminum are falling freely through water and for the finely-fragmented aluminum drops in the wake of the pressure shock that "triggers" the explosion. Vapor phase burning is predicted to be possible during the pre-mixture phase but not very likely during the trigger phase of a steam explosion. The implications of these findings in terms of the validity of the hypothesis that ignition may begin with the vapor phase burning of aluminum is discussed. Recently postulated, alternative mechanisms of underwater aluminum ignition are also discussed.

1.0 INTRODUCTION

The potential for explosions upon bringing hot molten material into contact with a volatile coolant have been recognized for some time now by the commercial nuclear power, metal and paper industries. Natural explosions produced by the interaction of magma and sea water is believed to be a component of some volcanic eruptions. In general, the postulated mechanism for such explosions is the fragmentation of the hot melt into fine drops or particulate with attendant rapid mixing and heat transfer between the melt and the coolant. Significant physical damage may occur when the rate of production of coolant vapor is so high that it is accompanied by the generation of a shock wave(s). This "physical or thermal explosion" is distinguished from a chemical explosion in which the energy is produced from chemical reactions. However, it is possible for both melt sensible heat and chemical reactions to contribute to the energy release associated with a hot melt/coolant interaction. An important example is the rapid mixing of high-temperature molten aluminum with water. If chemical energy is released the explosion could be much more damaging than if only the melt sensible heat were transferred to the coolant.

The aluminum water system as a potentially explosive pair is of great practical interest, as postulated severe accidents for existing and future production nuclear reactors involve the melting of aluminum in water. Also, the metals casting industry is concerned about their operations where molten aluminum and water are in close proximity. Much of the testing on molten aluminum/water explosions has, in fact, been supported by the metals casting industry. In 1957 Long [1] published the results of a study of explosions of molten aluminum in water. He spilled about 23 kg of molten, commercially pure aluminum into a water container. A total of 880 tests were conducted and involved variations in the diameter of the metal pour stream, the water depth and temperature, and the temperature of the melt, which ranged from 933 to 1173K. In classifying the intensity of the explosions observed, Long's evaluation was based on the extent of destruction of the water container. Many of the explosions were strong enough to break the steel water containers. Since a visible flash was never observed during the course of

an explosion, Long concluded that chemical reactions did not contribute to the explosive yield. Long also found that the aluminum/water pair would explode only when (1) a large fraction of the metal reached the bottom of the container in a molten state and (2) a trigger (pressure pulse) is produced at the bottom surface when it is covered by molten metal. Hess and Brondyke [2] repeated Long's pioneering experiments, except that the water containers were now instrumented with thermocouples. Very violent explosions accompanied by an intense light were observed when the inside surface of the container was coated with calcium hydroxide or rust. Since the measured maximum temperatures within the container exceeded that of the incoming metal, it was concluded that the most violent explosions involved chemical reactions. Hess and Brondyke postulated that "chemical or ignition-type vapor explosions" were initiated by a thermite reaction between the container bottom oxide-coated material and the aluminum. Indeed the temperature at the container bottom was observed to rise rapidly just prior to a catastrophic explosion event which destroyed the container. The authors believed that the thermite reaction locally raises the aluminum temperature from its initial temperature of about 1100K to the threshold temperature of 1450K required to initiate a rapid reaction between molten aluminum and water. Unfortunately, Hess and Brondyke did not convey to the reader the significance of the 1450K temperature level as an ignition condition.

The work of Long [1] and Hess and Brondyke [2] has indicated that the trigger mechanism for a vapor explosion is probably a pressure shock produced by the sudden conversion to steam of a thin layer of water trapped between the molten metal and the container bottom. Presumably, the trigger shock propagates through the melt and creates fresh metal surface, which is accompanied by rapid heat transfer and, perhaps, rapid chemical reaction between the metal and the water. A number of experiments were reported by Lemmon [3] to determine if aluminum/water explosions could be initiated artificially by the application of an explosive charge (detonator) to produce a pressure pulse. Indeed the transmission of strong shocks into the melt pour stream produced very violent explosions in which metal/water reactions occurred on the time-scale of the explosions. The experiments employed either aluminum-, glass- or coated steel-bottom water containers.

In all tests the metal was preheated to about 1300K. The metal mass varied between 4,5 and 12 kg of aluminum. No explosions were produced in the absence of an imposed pressure pulse in aluminum- or glass-bottom containers.

Similar violent explosions were observed during a recent test series conducted by Rightly and Beck [4] for the Department of Energy's Office of New Production Reactors. Six tests were performed in which melt masses from about 2 to 10 kg were dropped into room temperature water. The tests were carried out with aluminum alloy 6061 and 6063 melts in the initial temperature range: 1000 - 1544K. Two important observations were made by Rightly and Beck that distinguishes their work from the previously referenced studies. Their results seem to exhibit an aluminum-melt temperature threshold below which the chemical contribution to the vapor explosion energetics vanishes. This threshold appears to lie between 1000 and 1150K, since only a moderate vapor explosion followed the firing of the detonator when the melt temperature was 1000K whereas a catastrophic explosion with intense light emission was observed at a melt temperature of 1150K. The other important finding is that it is possible for an aluminum water vapor explosion to occur in free-fall in water (i.e., before the melt contacts the bottom of the container) without an artificially produced pressure shock. In one of Rightly and Becks' tests the detonators fired before the melt had entered the water, and yet a very energetic explosion was initiated just after the melt penetrated the surface of the water. It was concluded that local violent boiling served as a natural trigger in this test. This is a significant result, considering that Long [1] performed 880 tests without observing a vapor explosion before the melt contacted the container bottom and, presumably, trapped some underlying water. This difference in results could be due to the fact that in Long's tests the initial melt temperature was about 1100K whereas an initial melt temperature of 1500K was used in the naturally triggered Rightly-Beck test. However, Lemmon [3] heated the aluminum melts in his tests to about 1330K and never observed an explosion while the melt was freely falling through water unless an explosive device was used that imparted a strong pressure pulse to the system. It should be mentioned that Rightly and Beck gave no information on the time lag between the firing of the trigger and the aluminum melt entering the water. Perhaps

the test container was still "ringing" with reflected shocks that were strong enough to initiate the explosion after the melt entered the water. A particular weakness in the reporting by Lemmon [3] and by Rightly and Beck [4] is the absence of information on the position- and amplitude-time histories of the artificially produced trigger shocks.

A small-scale experimental program to study explosions in the aluminum water system is presently being carried out by Nelson et al. [5]. They have achieved reproducible small-scale physical vapor explosions. The explosions are initiated by the impingement of strong pressure shocks (> 20 atm) upon pure aluminum and aluminum alloy drops (~ 6 g) in free-fall in water. The pressure shocks are generated by an exploding wire technique. To date, in all of the tests but one the initial metal melt temperature was in the range 1300 - 1700K. Interestingly enough, a vigorous explosion was produced when the initial temperature of the melt drop exceeded approximately 1800K. An estimate of the explosion energy was made from a movie taken at high framing rates of the volume of the underwater bubble produced by the explosion. This estimate and the fact that the experimental apparatus was destroyed strongly suggest that aluminum combustion occurred together with the transfer of melt sensible heat.

It is clear from the experiments discussed in the foregoing that rapid aluminum oxidation (ignition) can take place underwater on an explosive time scale (~ 1 msec), even when the initial temperature of the aluminum melt is quite low (~ 1100K).* Since aluminum is known to form a very protective oxide layer at its surface, the question naturally arises as to the mechanism of aluminum ignition during a vapor explosion event. There seem to be only two ways in which underwater aluminum ignition followed by rapid oxidation can take place. These are: (1) the sudden exposure of a freshly formed, solid-oxide-free metal surface to steam or (2) the sudden transition to vaporization and burning of the aluminum some distance off the metal

---

*. It should be kept in mind, however, that the experimental evidence suggests that such an ignition probably requires a strong initiator, such as a blasting cap.

surface (vapor-phase burning) at a rate that prevents the steam from contacting the surface.

Just recently, some work has been carried out on theoretical determinations of ignition temperatures of aluminum submerged in water. Kuan and Buescher [6] performed an analysis that links the ignition temperature with the kinetic rate of oxidation of the metal in the vapor phase. The treatment is based on the generally accepted view that ignition will occur if the heat produced by the surface oxidation reaction exceeds the heat losses to such an extent that the metal temperature rise continues at an accelerating rate. The authors considered both metal evaporation and radiation heat losses and predicted a threshold temperature for aluminum ignition of 1684K. They pointed out that this prediction is in excellent agreement with test results reported by Higgins and Schultz [7] and obtained by injecting molten aluminum into water. No justification was given by Kuan and Buescher for their assumption of vapor phase burning. Their model ignores the limitation to the reaction rate due to the counter diffusion of steam and hydrogen in the region between the water and the reaction front. Furthermore, the model neglects convective heat losses from the metal surface which, as we shall see below, are much more important than radiative effects. Thus the reported agreement with experiment should be regarded as fortuitous.

Young and Nelson [8] adopted a steady-state stagnation flow theory for predicting the oxidation rate of spheres in film boiling due largely to Epstein et al. [9] and simplified by Pong [10]. The estimates of oxidation rate are based on either diffusional limitations in the steam/hydrogen film located between the metal surface and the water or oxidation kinetics beneath the metal surface. The authors postulated that during fragmentation of the melt and the subsequent violent boiling phase of a steam explosion the protective oxide layer is absent and the oxidation of the melt particles depends only on steam-hydrogen diffusion. The numerical results obtained by Young and Nelson [8] from Pong's model indicate that heat is generated at the surface of the aluminum sphere (drop) by oxidation at a lower rate than it is lost by convection and radiation when the drop temperature is less than 1100K. A net energy gain is predicted for temperatures above 1100K. This theoretical result appears to explain the observed [4], approximately

1100K threshold below which chemical reactions do not contribute to the energetics of an aluminum/water explosion. An essential aspect of the water/reactive metal-drop system is that the net influx of steam to the drop strongly influences the profiles of temperature and species concentration within the steam/hydrogen film, in addition to introducing energy and mass transport from and to the drop, respectively, by mass motion (i.e., "suction"). These important effects were incorporated in the original oxidation model by Epstein et al. [9] but, unfortunately, were eliminated in the simplifications proposed by Pong [10]. The omission of chemical suction effects results in significant underestimates of the drop oxidation and heat loss rates. As demonstrated below, the complete (numerically exact) stagnation flow model does not exhibit the temperature threshold predicted by Young and Nelson [8] in the limit of oxidation by steam transport.

As mentioned in the foregoing, Kuan and Buescher [6] assumed that the aluminum drop is heated to ignition by rapid vapor phase burning, while Young and Nelson [8] predicted a temperature threshold for aluminum drops in water under the assumption that the ordinarily very protective oxide scale vanishes from the aluminum melt surface during an energetic interaction, thereby allowing surface oxidation at a rate proportional to diffusion-limited steam uptake. Clearly it is important to determine which one of these mechanisms can explain the presence of chemical reactions during an aluminum/water explosion. The main goal of the work reported herein was to examine vapor phase burning as a mechanism of ignition. The vapor phase burning mechanism is appealing because it allows us to bypass the difficult question of the stability of the protective oxide layer. As a result of the present study it now appears that vapor phase burning may be responsible for the onset of ignition, but sustained ignition (or chemical reaction) probably occurs by surface oxidation. This conclusion leaves open the possibility that the surface reaction may play the predominant role throughout the ignition process. Thus, while our emphasis is on the transition to vapor phase burning, calculations of the heating of aluminum spheres by steam transport-controlled surface oxidation are also included in the hope that reactive sphere heat-balance considerations can provide an alternative explanation for the observed temperature thresholds for ignition. As

in the work of Young and Nelson [8], these thermal-runaway- type calculations are made under the assumption that the protective properties of the oxide surface layer are somehow suppressed during the course of a steam explosion. Unfortunately, as already mentioned, steam transport-controlled aluminum drop heat-up calculations can not by themselves explain ignition and, therefore, the important work on the question of the stability of the oxide layer really lies ahead. We plan to address this question in the very near future.

We begin the next section (Section 2.0) with a discussion of ignition of aluminum in gaseous atmospheres. Our purpose here is to introduce the reader to an available criterion for the transition to vapor phase burning and to build some confidence in this criterion by comparing its predictions with measured threshold temperatures for ignition of aluminum in oxygen-containing gases. In Section 3.0 we exploit an available theoretical model of forced-convection film boiling which includes most of the important coupled fluid mechanical and transport processes that occur within the steam film that envelopes the hot, molten aluminum particle. This model, together with the criterion presented in Section 3.0, enables rational predictions of the conditions under which vapor phase burning of aluminum submerged in water is possible. The film boiling model is used once again in Section 4, this time to search for potential thresholds to droplet self-heating by diffusion-limited surface oxidation under steam explosion conditions. A byproduct of these calculations is the conclusion that steam-transport limited oxidation can transform a molten aluminum drop with a bare surface into a microsphere of oxide (Al_2O_3) on the time scale of a steam explosion.

2.0 VAPOR PHASE BURNING OF METAL WIRES AND DROPS IN REACTANT GASES

2.1 Vapor Phase Burning Transition Condition

Most of what is known about the vapor phase burning of metals comes from studies of metal combustion in oxygen-containing gases. Baker and Simms [11] recently reviewed the available data on the reactions of aluminum and aluminum alloys with water, steam and reactive gaseous atmospheres. Their review contains an excellent summary of the observations of aluminum burning in the vapor phase. The available data indicates that aluminum burning in oxygen-inert gas mixtures is complex in that it may involve simultaneous vapor phase and surface reactions. Characteristic of the former mode of combustion is a high rate of burning, the presence of a luminous reaction zone located some distance from the metal surface, and the formation of "oxide smoke" consisting of small particles in the submicron range. Some of the observations reviewed in [11] indicate the onset of rapid aluminum burning (ignition) above the melting temperature of aluminum oxide (2315K). Apparently the oxide scale loses its protectiveness once it becomes molten. However, reported ignition temperatures of aluminum wires or drops in reactive gases are as low as 1700K [12]. Again, it is not clear whether these ignitions correspond to transitions from slow surface burning to vapor phase burning or to a steep increase in the rapid surface oxidation rate due to suddenly exposing a bare metal surface to oxygen-containing gas. Nevertheless, many authors believe that the ignition of aluminum is a transition to vapor phase burning.

A necessary but not sufficient condition for vapor phase burning has been proposed by Glassman [13]. Since the flame temperature cannot exceed the boiling point of the oxide, he suggested that in order for vapor phase burning to occur the boiling point of the oxide must exceed the boiling point of the metal. This condition follows from the requirement that heat flow from the reaction zone (flame) to the metal surface to sustain metal vaporization and, therefore, the vapor phase burning process. Aluminum satisfies the Glassman condition.

A sufficient condition for the breakdown of the vapor phase burning regime of metals has been provided by the work of Turkdogan et al. [14]. At temperatures where the vapor pressure of the metal is appreciable and the metal is exposed to an oxygen-containing gas stream of low oxygen concentration, metal atoms vaporize from the surface and diffuse into the boundary layer up to a certain distance where they encounter and react with oxygen molecules which diffuse into the boundary layer from the gas stream. At the reaction front, metal atoms and oxygen molecules form embryos of solid (or liquid) metal oxide which are carried away by convection and thermophoretic transport. This picture describes the vapor phase burning mechanism. When the oxygen concentration in the bulk stream is gradually increased, the rate of metal evaporation must increase to keep up with the increase in the incoming oxygen diffusion rate. In order for the metal evaporation rate to increase, the reaction front moves closer to the metal surface. Turkdogan et al., reasoned that there is an upper bound to the bulk stream oxygen concentration above which the reaction-enhanced vaporization rate exceeds the maximum, vacuum vaporization rate of the metal per unit area of metal surface, $\dot{m}_{vac}$, given by the Hertz-Langmuir equation

$$\dot{m}_{vac} = \frac{P_{eq,m}(T_m)}{(2\pi \bar{R} T_m / M_m)^{1/2}} \qquad (2\text{-}1)$$

where $P_{eq,m}(T_m)$ is the vapor pressure of the metal at the metal temperature T_m, $\bar{R}$ is the ideal gas constant and M_m is the molecular weight of the metal. Turkdogan et al. showed that when the metal vaporization rate achieves the vacuum vaporization value, the reaction front moves to within a distance of the metal surface comparable to the prevailing inert gas molecular mean-free-path. Thus when the oxygen content in the bulk stream is increased to a value that causes the evaporation rate of the metal to exceed $\dot{m}_{vac}$, the mechanism of vapor phase burning breaks down; that is, the diffusive supply of oxygen can no longer be accommodated by the maximum possible rate of metal evaporation and oxygen reaches the surface.

Indeed, Turkdogan et al. [14] experimentally demonstrated that the evaporation rate of molten metals (Cu, Ni, Fe, Co, Cr and Mn) heated to a predetermined temperature can be made to approach the vacuum evaporation

rate by gradually increasing the bulk stream oxygen concentration. Any attempt to increase the evaporation rate beyond this point by further increases in the oxygen concentration resulted in a sudden and significant decrease in the metal vaporization rate, owing to a change in reaction regime from vapor phase burning to surface burning. An alternative interpretation of the Turkdogan et al. [14] vapor-to-surface burning transition criterion that is more useful for present purposes is that for a fixed free-stream oxygen content the metal temperature must exceed some critical value $T_{m,cr}$ in order for the metal vaporization rate to be high enough to "consume" all the incoming oxygen and thereby support a vapor phase reaction zone. It is important to recognize that vapor phase burning does not necessarily occur upon heating the metal above $T_{m,cr}$; it may be delayed or suppressed by a pre-existing protective oxide layer. However, upon cooling the metal below $T_{m,cr}$, extinction of the flame must inevitably occur.

At the reaction front the metal vapor Me and the oxidizer gas Ox react forming metal oxide MeO and inert gas I in accord with the stoichiometry

$$Me(g) + nOx \rightarrow MeO + sI \tag{2-2}$$

where n is the moles of oxidizer gas removed per mole of metal vapor reacted and s is the moles of inert gas produced per mole of metal vapor reacted. Some oxidizer gases of practical interest are O_2, H_2O, and CO_2. An implicit equation for the critical temperature that defines the reaction regime transition follows from the overall stoichiometry, Eq. (2-2) [2]:

$$\dot{m}_{vac}(T_{m,cr}) = - \frac{M_m}{M_o n} \cdot \dot{m}_o \tag{2-3}$$

Since the distance between the vapor phase reaction zone (flame) and the metal surface is much smaller than the boundary layer thickness at incipient flame extinction, the flux of oxidizer gas $\dot{m}_o$ may be estimated from boundary layer theory under the assumption that the reaction front is located at the metal surface.

2.2 Oxidizer Gas Transport Model

It is prudent to compare Eq. (2-3) with the available data on the transition to vapor phase burning of aluminum exposed to an oxidizer gas, a comparison which has apparently not previously been made. To illustrate the reaction regime transition criterion in gaseous environments, we first consider the transport of an oxidizer gas through a steady-state one-dimensional thin gas-film representation of the boundary layer adjacent to the vaporizing metal (see Fig. 2-1). Later on in this subsection we will extend the model to transport in real boundary layers. The oxygen species is assumed to diffuse according to Ficks' pseudo-binary law. Thus the oxygen species conservation equation in the film of thickness δ is

$$\dot{m} \frac{dY}{dy} = \rho D \frac{d^2Y}{dy^2} \tag{2-4}$$

where $\dot{m}$ is the total mass flux of gas (inert + oxidizer) normal to the metal surface, y is the distance measured from the metal surface (or reaction front), ρ is the total gas density, and D is the binary Fick Diffusion coefficient for the oxidizer gas species. In writing Eq. (2-4) a constant average value has been assumed for the product ρD.

Integrating Eq. (2-4) once yields

$$\dot{m}Y - \rho D \frac{dY}{dy} = \dot{m}_o = \text{const} \tag{2-5}$$

which states that the oxidizer mass flux $\dot{m}_o$ is comprised of a diffusive and convective contribution. At the reaction front we have the boundary condition

$$Y = 0 \quad \text{at} \quad y \approx 0 \tag{2-6}$$

At the outer edge of the film (boundary layer)

$$Y = Y_\infty \quad \text{at} \quad y = \delta \tag{2-7}$$

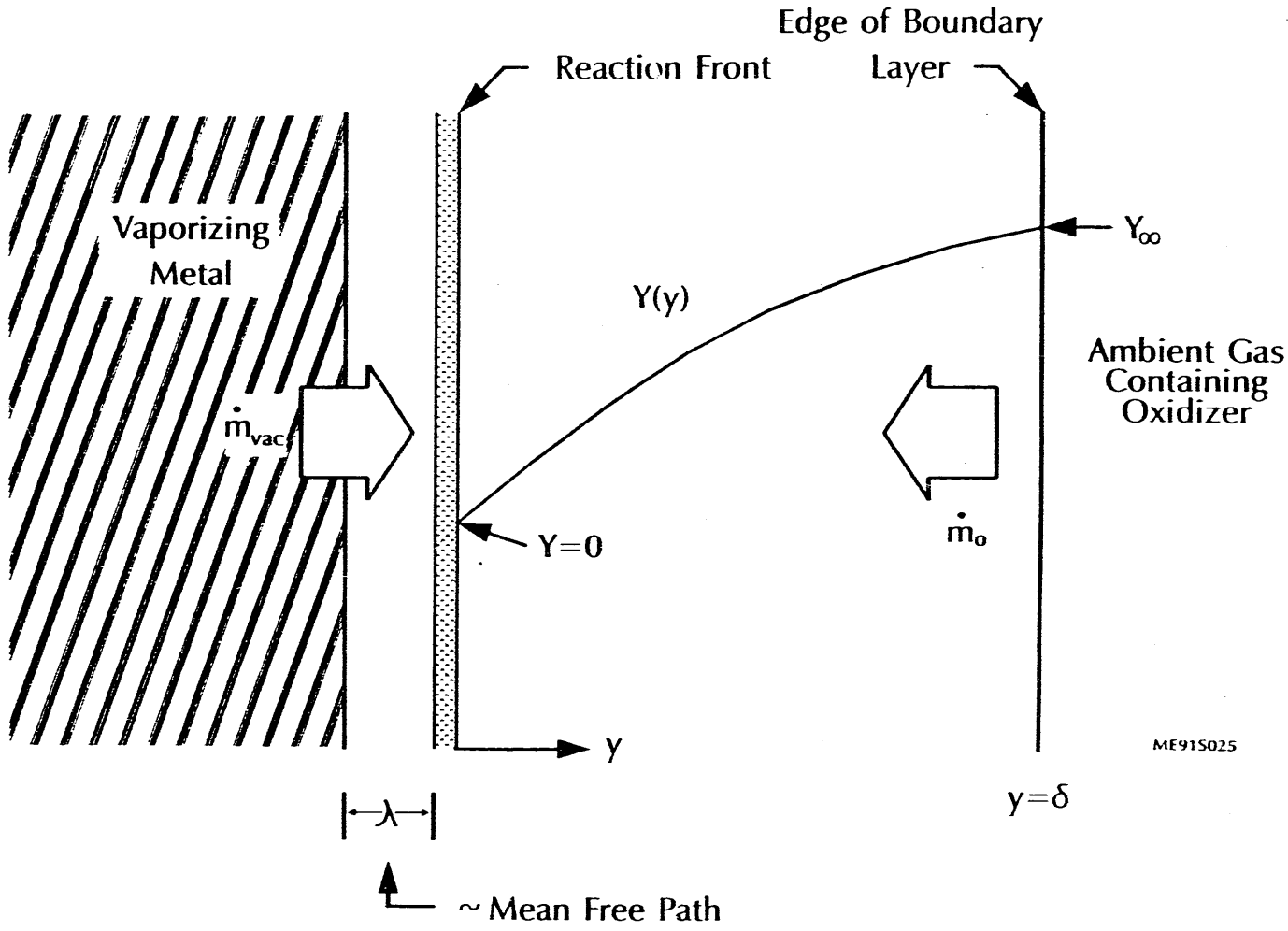

Figure 2-1 Thin-film model of boundary layer with reaction front supplied by metal vapor at the maximum possible rate; i.e., at incipient break down of vapor phase burning regime.

Integrating Eq. (2-5) once more and applying boundary conditions (2-6) and (2-7) gives

$$\frac{\dot{m}\delta}{\rho D} = \ln\left[1 - \frac{\dot{m}\, Y_\infty}{\dot{m}_o}\right] \tag{2-8}$$

Now the total hydrodynamic mass flux in the boundary layer equals the sum of the oxidizer gas mass flux and inert product gas mass flux; that is

$$\dot{m} = \dot{m}_o + \dot{m}_I \tag{2-9}$$

It should be noted that, in addition to the product gas inert species I, the ambient inert gas is also present in the boundary layer. However, since there must be no net mass flow of this inert species normal to the metal it does not contribute to the total mass flux $\dot{m}$. From the stoichiometry given by Eq. (2-2), $\dot{m}_o$ and $\dot{m}_I$ must obey the relation

$$\frac{\dot{m}_I}{sM_I} = -\frac{\dot{m}_o}{nM_o} \tag{2-10}$$

Combining Eqs. (2-8) through (2-10) yields

$$\frac{\dot{m}_o\delta}{\rho D} = \frac{\ln\left[1 - \left[1 - \frac{sM_I}{nM_o}\right]Y_\infty\right]}{1 - \frac{sM_I}{nM_o}} \tag{2-11}$$

The logarithm enters Eq. (2-11) because the hydrodynamic flow induced by the diffusion process causes increasing curvature of the oxidizer gas mass fraction profile, Y(y), as the mass transfer rate increases. When this rate is low, Eq. (2-11) reduces to

$$\frac{\dot{m}_o\delta}{\rho D} = -Y_\infty \tag{2-12}$$

Thus at low values of Y_∞ the mass flux of the oxidizer gas is directly proportional to Y_∞ because the curvature of the "Y"-profile is negligible. From Eqs. (2-11) and (2-12), the ratio of the oxidizer-gas mass flux at the reaction front under high-mass-flux conditions to that at low-mass-flux is given by

$$\frac{\dot{m}_o}{\dot{m}_{o,low}} = \frac{\ln\left[1 - \left[1 - \frac{sM_I}{nM_o}\right]Y_\infty\right]}{\left[1 - \frac{sM_I}{nM_o}\right]Y_\infty} \tag{2-13}$$

While the above equation has been derived from one-dimensional film theory, it is well known from the work of Spalding [15] and others that Eq. (2-13) correctly accounts for the effect of high mass-transport rates in real boundary layers.

The oxidizer-gas mass-transfer rate to a reaction front of arbitrary shape at low transfer rates can be expressed in terms of the Sherwood number as

$$\dot{m}_{o,low} = \frac{\rho D Y_\infty}{L} \cdot Sh \tag{2-14}$$

where L is the characteristic dimension of the reaction front or, equivalently, the dimension of the metal melt beneath the reaction front. From Eqs. (2-1), (2-3), (2-13) and (2-14) we have the following implicit expression for the critical metal temperature that separates surface burning from vapor phase burning:

$$\frac{P_{eq,m}(T_{m,cr})}{(2\pi \bar{R} T_{m,cr}/M_m)^{1/2}} = -\frac{M_m \rho D Sh}{L(nM_o - sM_I)} \cdot \ln\left[1 - \left[1 - \frac{sM_I}{nM_o}\right]Y_\infty\right] \tag{2-15}$$

2.3 Prediction of Vapor Phase Regime for Burning Aluminum Wires and Drops

To demonstrate the use of Eq. (2-15) for $T_{m,cr}$, we first consider the combustion of a horizontal aluminum wire in an oxygen-argon mixture. This

system was studied experimentally by Kuehl [12]. In this case only solid Al_2O_3 is formed by the reaction

$$Al(\ell) + \frac{3}{4} O_2(g) = \frac{1}{2} Al_2O_3(s) \tag{2-16}$$

Thus there is no inert product gas, s = 0 in Eq. (2-15), and the criterion for vapor phase burning simplifies to

$$\frac{P_{eq,m}(T_{m,cr})}{(2\pi \bar{R} T_{m,cr}/M_m)^{1/2}} = - \frac{M_m \rho D Sh}{L\, n M_o} \ln(1 - Y_\infty) \tag{2-17}$$

The molecular weights $M_m = 27.0$ and $M_o = 32$ for aluminum and oxygen gas, respectively. The Sherwood number is estimated from the correlation of Nakai and Okazaki [16] for natural convection heat transfer from a horizontal circular cylinder at small Grashof numbers, Gr. Using this correlation and the heat-mass transfer analogy we obtain the following inverse relationship between Sh and Gr:

$$Gr = \frac{E}{Sh} \cdot e^{-3/Sh} \tag{2-18}$$

The parameter E is a function of the Schmidt number ($Sc = \nu/D$)

$$E = \frac{3.1(Sc + 9.4)^{1/2}}{Sc^2} \tag{2-19}$$

and the Grashof number is defined in terms of the radius R of the cylinder (wire); namely

$$Gr = \frac{g\beta_T \Delta T R^3}{\nu^2} \tag{2-20}$$

Thus, for this case, the dimension L in Eq. (2-17) must be identified with the radius of the wire. In Eq. (2-20) β_T and ν are the coefficient of thermal expansion and the kinematic viscosity of the gas mixture, g is the gravitational constant, and $\Delta T = T_m - T_\infty$ is the temperature difference between the metal (wire) and the ambient.

As with the properties D and ρ, it is assumed that suitable constant average property values can be defined for β_T and ν. Since the molecular weight and physical properties of argon are close to those of oxygen, the properties ρ and absolute viscosity μ are based on argon gas. The property μ for argon is estimated from the following formula contained in [17]:

$$\mu = \frac{1.087 \times 10^{-6}\ T_r^{0.5837}}{1 + 97.9/T_r}\ , \quad \frac{kg}{m \cdot s} \tag{2-21}$$

The density is calculated from the ideal gas law

$$\rho = \frac{P_\infty\ M_{Ar}}{\bar{R}\ T_r} \tag{2-22}$$

where $M_{Ar} = 39.94$ is the molecular weight of argon. In the above equations T_r is the reference temperature for physical property evaluation and is given by the so-called film temperature*:

$$T_r = \frac{1}{2}(T_m + T_\infty) \tag{2-23}$$

With this reference temperature, Sparrow and Gregg [18] have shown that the results of constant-property analysis approximately coincides with variable-property natural convection calculations when the coefficient of thermal expansion is calculated at T_∞, thus

$$\beta_T = \frac{1}{T_\infty} \tag{2-24}$$

---

*. Strictly speaking, the metal temperature T_m in Eq. (2-23) should be replaced by the temperature T_f at the reaction front. However, by considering an energy balance "jump" condition across the reaction front we find that the difference $T_f - T_m$ is less than 300K when, say, $T_m = 2000K$ and the flame is at the incipient extinction condition, $T_m = T_{m,cr}$. The difference $T_f - T_m$ decreases with decreasing T_m.

The argon-oxygen binary diffusion coefficient D was estimated from the Chapman-Enskog formula for nonpolar molecule pairs. The result is

$$P_\infty D = 1.23 \times 10^{-4}\, T_r^{1.7} \quad , \quad \frac{Pa \cdot m^2}{s} \tag{2-25}$$

Finally, the formula for the vapor pressure of aluminum is taken from Ref. [19] and is

$$P_{eq,Al} = \frac{2.79 \times 10^{14}}{T_m}\, e^{-\frac{3.772 \times 10^4}{T_m}} \tag{2-26}$$

Equation (2-17) was solved graphically by plotting the left-hand-side of the equation and seeking the intersection with its right-hand-side for a fixed value of Y_∞. The theoretical result is shown in Fig. 2-2 for a 0.51-mm diameter aluminum wire. Also given in Fig. 2-2 are the minimum ignition temperatures measured by Kuehl [12]. These data points were obtained at low, subatmospheric pressures (~ 0.03 atm). As the pressure was increased to 1.0 atm the ignition temperature was observed by Kuehl to increase to approximately 2300K, close to the melting point of aluminum oxide. No further increase in ignition temperature was noted with further increases in system pressure. Kuehl reasoned that at low ambient pressures the metal surface is readily exposed to the reactive gas, since the oxide scale should fail when the vapor pressure of the metal exceeds the ambient pressure. These experimental results combined with Eq. (2-17) for the minimum temperature for vapor phase oxidation appear to be consistent with the idea that ignition takes place through a vapor phase reaction. Note that the comparison in Fig. 2-2 of the predicted $T_{m,cr}$ curve with the measured ignition temperatures at low pressures is a valid comparison since the theoretical results are insensitive to the prevailing pressure.

It should be mentioned that the data point at $Y_\infty = 1.0$ in Fig. 2-2 was reported by Kuehl for a pure oxidizer environment. An examination of Eq. (2-15) or (2-17) indicates that the theory breaks down for metals burning in pure oxidizer ambients ($Y_\infty = 1.0$) and in the absence of a chemically produced product gas ($s = 0$). Under these conditions the metal surface is

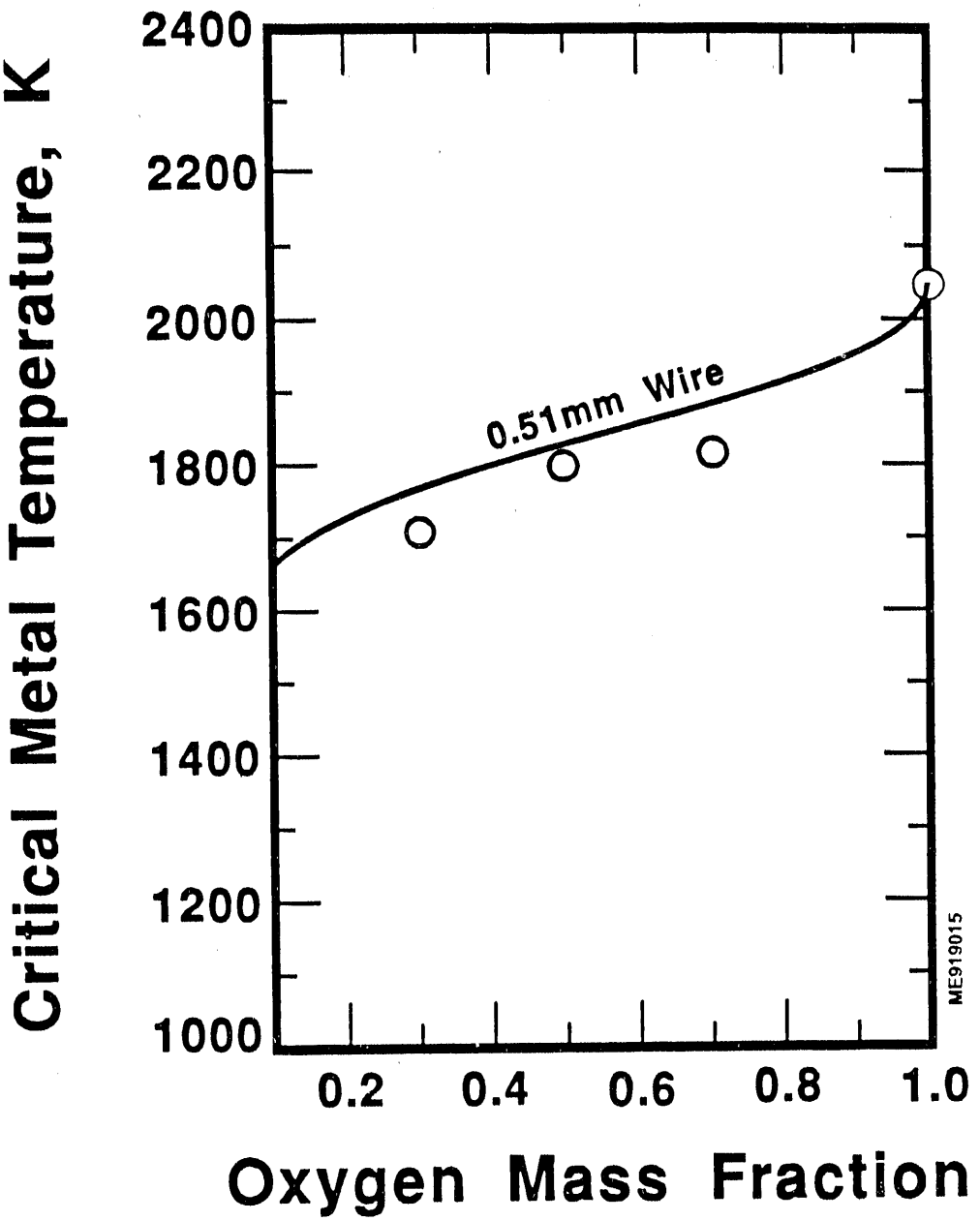

Figure 2-2 Predicted critical (minimum) metal temperature for vapor phase burning of a horizontal 0.51-mm diameter aluminum wire in oxygen-argon mixtures; comparison with measured minimum ignition temperatures [12].

predicted to be incapable of supporting a vapor phase reaction zone at any surface temperature below the boiling point of the metal (2740K for aluminum). However, the slightest amount of inert impurity can, according to the theory, allow vapor phase burning at metal temperatures significantly below the metal boiling point. This sensitivity to small amounts of ambient inert gas causes obvious difficulties in comparing theory with experiment in nearly pure oxidizer ambients.

Figure 2-3 shows the predicted critical (minimum) metal temperature for vapor phase burning as a function of the ambient oxygen mass fraction for a 10-mm diameter aluminum sphere in an oxygen-nitrogen gas mixture. This curve was constructed from Eq. (2-17) and the Raithby and Hollands [20] correlation for diffusive transport in natural convection around a sphere; namely,

$$Sh = 2.0 + 0.56\left(\frac{Sc^2 Gr}{Sc + 0.840}\right)^{1/4} \qquad (2\text{-}27)$$

All the physical properties of the gas mixture were taken to be those of air and obtained from the tables that appear in Ref. [21]. Studies by Wilson et al. [22] in which molten aluminum spheres, approximately 10 mm in diameter, were produced in air by the levitation method showed delayed ignitions. The ignition delay time increased with decreasing melt temperature. The ignition of aluminum at 1873K required a waiting time of about 18 min. This was the lowest ignition temperature reported in this study and it is about 200K above the predicted minimum ignition temperature curve based on vapor phase burning (see Fig. 2-3).

Additional ignition temperature measurements have been reported by Merazanov et al. [23] and Kuehl [12] using electrically heated aluminum wires in pure oxygen, carbon dioxide and steam atmospheres. For reasons mentioned previously, it is difficult to achieve a meaningful comparison between theory and experiment for nearly pure oxygen environments. This is not the case with nearly pure oxidizers such as steam or carbon dioxide. Because of the production of inert product gas at the reaction front, in accord with the reactions

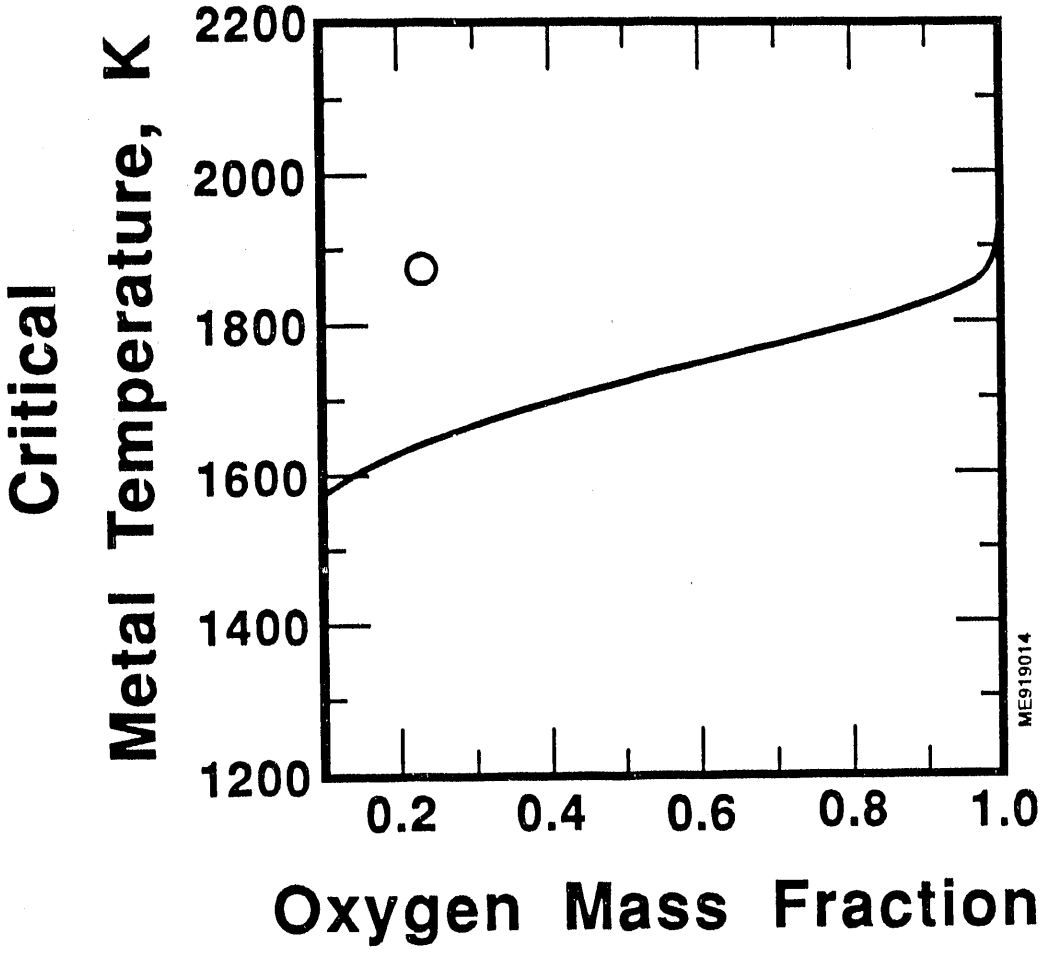

Figure 2-3 Predicted critical (minimum) metal temperature for vapor phase burning of 10-mm diameter aluminum spheres in oxygen-nitrogen mixtures; comparison with measured minimum ignition temperature in air [22].

$$Al(\ell) + \frac{3}{2} H_2O(g) \rightarrow \frac{1}{2} Al_2O_3(s) + \frac{3}{2} H_2(g) \qquad (2\text{-}28)$$

$$Al(\ell) + \frac{3}{2} CO_2(g) \rightarrow \frac{1}{2} Al_2O_3 + \frac{3}{2} CO(g) \qquad (2\text{-}29)$$

a steady-state counter flux transport process is established and constant pressure can be maintained at the reaction front. By comparing these reactions with the general stoichiometric relation, Eq. (2-2), we find n = s = 3/2. Thus in the limit $Y_\infty \rightarrow 1.0$, Eq. (2-15) for the critical temperature for transition to vapor phase burning becomes

$$\frac{P_{eq,m}(T_{m,cr})}{(2\pi \bar{R} T_{m,cr}/M_m)^{1/2}} = - \frac{2M_m \rho D Sh}{3L(M_o - M_I)} \ln\left(\frac{M_I}{M_o}\right) \qquad (2\text{-}30)$$

For predicting $T_{m,cr}$ for aluminum wires burning in CO_2 (M_o = 44.01, M_I = 28.01), the properties ρ, D, Sc were estimated from the following formula:

$$\rho = \frac{M_{mix} P_\infty}{\bar{R}\, T_r} \qquad (2\text{-}31)$$

$$P_\infty D = 1.211 \times 10^{-4} T_r^{1.672} \quad , \quad \frac{Pa \cdot m^2}{s} \qquad (2\text{-}32)$$

$$\mu = \frac{2.148 \times 10^{-6} T_r^{0.46}}{1 + \frac{290.0}{T_r}} \quad , \quad \frac{kg}{m \cdot s} \qquad (2\text{-}33)$$

Equation (2-31) is the ideal gas law. The molecular weight M_{mix} of the CO-CO_2 mixture is based on the reference oxidizer mass fraction 1/2 Y_∞, which results in M_{mix} = 34.23. Equation (2-32) is an approximate formula for the diffusion coefficient, based on predictions obtained from the Chapman-Enskog theory. The viscosity of the mixture, given by Eq. (2-33), is actually the viscosity of pure CO_2. Since the viscosities of CO and CO_2 are similar, this assumption is expected to be quite reasonable. For aluminum wires burning in steam, we have M_o = 18.02 and M_I = 2.016. The values of the H_2-H_2O gas mixture properties actually used to calculate $T_{m,cr}$ for wires burning in steam are presented later on when we discuss the oxidation and

vapor phase burning of aluminum under water. The Sherwood number is calculated from Eq. (2-18) for pure natural convection around a horizontal wire. The theoretical results are listed in Table 2-1, together with the experimentally determined ignition temperatures.

Table 2-1

THEORETICAL AND MEASURED CRITICAL

TEMPERATURE FOR ALUMINUM WIRE IGNITION

REFERENCE	OXIDIZER GAS	WIRE DIAMETER	MEASURED	PREDICTED
[12]	H_2O	0.51 mm	1700K	1775K
[23]	CO_2	0.05 mm	2300K	2020K

Clearly, Fig. 2-3 and Table 2-1 do not indicate near perfect agreement between measured ignition temperatures and the predicted minimum metal temperatures required to support vapor phase burning. Equation (2-3), however, certainly provides a reasonable lower bound to the ignition temperature and shows rough agreement as to trends, as it predicts the observed increase in the ignition temperature with increasing ambient oxidizer concentrations (Fig. 2-2) and decreasing aluminum drop (wire) sizes (Table 2-1). Thus it would appear that ignition of aluminum melts in quiescent, reactive gaseous atmospheres is compatible with the notion of a transition from a slow surface reaction to a fast gas-phase reaction. It is tempting to inquire if the transition to vapor phase burning can explain observed aluminum ignitions under water, especially during the violent aluminum/water contact modes in advance of a steam explosion. Underwater aluminum oxidation is considered in the next section.

3.0 HEAT AND MASS TRANSPORT MODEL FOR UNDERWATER ALUMINUM OXIDATION/BURNING

Once molten aluminum enters the water it is reasonable to suppose that the water is separated from the hot aluminum surface(s) by a film of steam, since the temperature of the aluminum melt is much greater than the saturation temperature of the water. Once established, the film provides a medium for the counter flux transport of steam and hydrogen gas. The heat flux from the molten aluminum surface to the water produces steam which diffuses to the surface or, in the case of incipient vapor phase burning, to the reaction front a few gas mean-free paths from the surface, and reacts there to form product hydrogen gas which diffuses away from the surface. The physical situation of interest is one in which the molten aluminum surface is in motion relative to the surrounding liquid. Thus consideration should be given to film-boiling in forced-convection boundary layer flow where gravity forces are negligible.

Epstein et al. [9] formulated a steady-state theory of forced convection film boiling from a surface undergoing a chemical reaction with the evaporated liquid based on the mass, momentum and energy equations for axisymmetric stagnation flow. The value of this model for present purposes is enhanced when one recognizes that the stagnation point behavior is likely to be dominant in determining the overall heat and mass transport rates on a translating blunt body (molten ligament or drop). Indeed, the stagnation flow model has already proved to be quite useful in correlating heat transfer data for forced convection film boiling from inert spheres and cylinders [24]. In Ref. [9] the predictions of the two-phase (steam/water) stagnation flow model with surface reaction were compared with the measurements reported by Crooks et al. [25] and Baker and Just [26] of the final extent of oxidation of initially molten zirconium spheres oxidized while falling freely through water. The agreement between the theory and the experimental trends was quite satisfactory.

Here we adopt the Epstein et al. [9] model of film boiling on a reactive surface. It is convenient to subdivide the presentation of the model into two parts: one dealing with a steady-state system in which the surface temperature of the aluminum melt is held constant and the rate of oxidation (burning) is limited by the rate at which steam is transported across the hydrogen-steam film by simultaneous convection and Fick diffusion, and the second dealing with the quasi-steady oxidation heating of an aluminum sphere in water when the rate of reaction at the aluminum surface is completely gas-film transport controlled. The former situation will allow us to readily illustrate the conditions required for vapor phase burning as well as comment on previous models of aluminum ignition in water, while the latter will enable us to determine if the reactive sphere energy balance alone leads to an ignition condition and to gain an appreciation for the oxidation time scales involved under steam explosion conditions.

3.1 Steady-State Stagnation-Flow Film Boiling Model for Prediction of Transition to Vapor-Phase Burning of Aluminum in Water

Figure 3-1 shows a sketch of the physical model and coordinate system of interest for predicting the minimum metal temperature consistent with vapor-phase burning. We consider a hot metal surface placed normal to a liquid (water) flow which has a uniform constant velocity, V_∞ at infinity. The temperature of the metal surface, T_m, is sufficiently high so that the metal surface is separated from the liquid by a continuous gaseous film. The film is divided into two sublayers by a reaction front located a few inert product-gas mean-free paths from the metal surface. Only steam and hydrogen gas co-exist between the front and the vaporizing water surface. Only metal (aluminum) vapor and hydrogen exists between the vaporizing aluminum surface and the reaction front. Of course, the hydrogen gas does not interfere with the vacuum vaporization rate of the metal in the highly rarefied environment between the metal surface and the reaction front. The temperature of the liquid at infinity is T_∞ which may be lower or higher than the temperature at the liquid surface (see Ref. [9]). In addition to

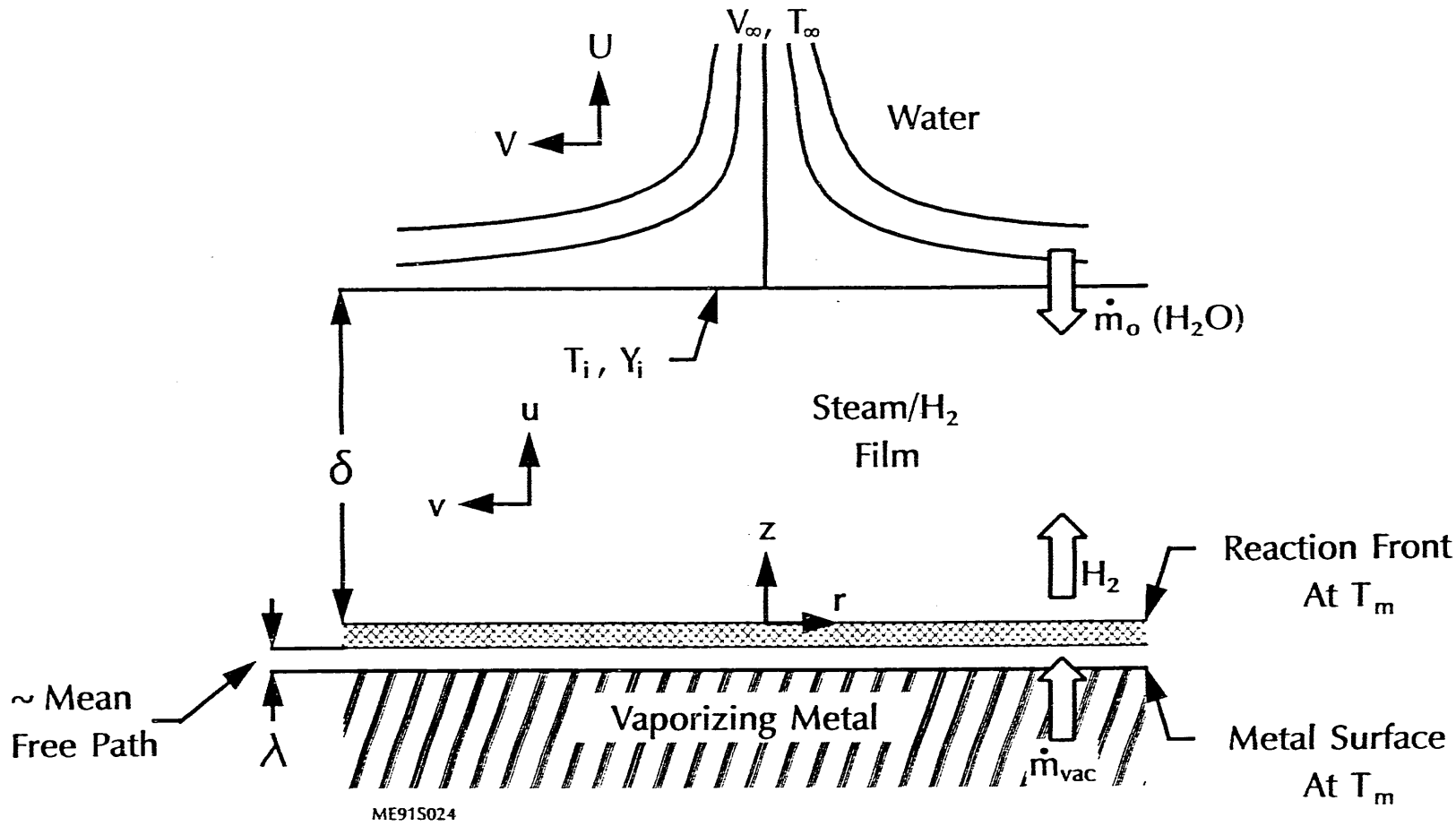

Figure 3-1 Stagnation flow film-boiling model with vapor phase chemical reaction supplied by metal vapor at the maximum possible rate, i.e., at incipient break down of vapor phase burning regime.

our assumption of laminar, steady axisymmetric stagnation flow, the following additional simplifications are introduced:

1. At the reaction front, the aluminum vapor and the steam meet in accord with the stoichiometry expressed by Eq. (2-28). The particles of oxide $Al_2O_3(s)$ formed at the reaction front are removed by convection, and form an aerosol that is dilute enough so that the velocity and temperature profiles in the steam/hydrogen film do not appreciably change from those predicted in the absence of chemical reaction.

2. The reaction front is so close to the metal surface that the boundary conditions for the steam/hydrogen velocity and temperature fields may be assumed to be those for the case where the reaction takes place at the metal surface. Again, we assume that the flame front temperature is prevented from significantly exceeding the metal temperature at the reaction front extinction condition (see footnote on page 2-9).

3. Suitable constant average values for the transport properties for the steam/hydrogen film and for the boundary layer in the surrounding water may be defined.

4. The processes of thermal diffusion and diffusional conduction are ignored. It should be noted that their effects are not insignificant in gas mixtures with both large molecular weight differences, such as hydrogen-steam mixtures, and large temperature gradients. However, the task of obtaining numerical solutions that include thermal diffusion and diffusional conduction is a formidable undertaking and for the time being is regarded as an interesting and important extension of the work presented herein.

5. The radiation heat flux from the reaction front (or, equivalently, metal surface) to the steam-water interface is estimated with the Stefan-Boltzmann law

$$\dot{q}_{rad} = e\sigma T_m^4 \qquad (3\text{-}1)$$

with back radiation from the relatively cold liquid surface regarded as negligible. It is assumed that thermal radiation is neither absorbed nor emitted in the steam-hydrogen film.

6. The steam mass fraction is set equal to zero at the reaction front as a result of the assumption that gas phase diffusion within the steam/hydrogen domain controls the reaction.

Subject to these assumptions, the two-phase stagnation flow film-boiling model for the steam film domain and surrounding water is identical to that of Epstein et al. [9] for film boiling on a reactive surface. From this work we know that the two-dimensional, axisymmetric stagnation flow velocity field equations can be made one-dimensional by introducing the position coordinate and dimensionless velocity components

$$\xi = (2a_\ell/\nu_\ell)^{1/2} z \quad , \quad U = a_\ell r F'(\xi) \quad , \quad V = -(2a_\ell \nu_\ell)^{1/2} F(\xi) \qquad (3\text{-}2)$$

for the liquid boundary layer, and

$$\eta = (2a/\nu)^{1/2} z \quad , \quad u = arf'(\eta) \quad , \quad v = -(2a\nu)^{1/2} f(\eta) \qquad (3\text{-}3)$$

for the vapor (steam/hydrogen) film. The constants a_ℓ and "a" in these equations are the so-called stagnation point velocity gradients for the liquid and vapor film regions, respectively:

$$a_\ell = \frac{3V_\infty}{2R} \quad , \quad a = \left(\frac{\rho_\ell}{\rho}\right)^{1/2} a_\ell \qquad (3\text{-}4)$$

Note that these relations for a_ℓ and "a" allow us to relate the stagnation flow analysis to the chemical reaction and flow conditions at the leading surface of a metal sphere. The primes in Eqs. (3-2) and (3-3) denote differentiation with respect to the dimensionless position coordinates ξ and η, respectively. The temperature profiles in the liquid and steam film and the steam mass fraction profile in the steam film are made dimensionless by introducing the definitions

$$\phi = \frac{T(\xi) - T_i}{T_\infty - T_i} \quad , \quad \theta = \frac{t(\eta) - T_m}{T_i - T_m} \quad , \quad \omega = \frac{Y(\eta)}{Y_i} \tag{3-5}$$

With the transformations given by Eqs. (3-2) through (3-5), the two-region boundary layer equations are reduced to the following well-known forms for stagnation flow:

$$F''' + FF'' + \tfrac{1}{2}(1 - F'^2) = 0 \tag{3-6}$$

$$\phi'' + Pr_\ell F\phi' = 0 \tag{3-7}$$

for the liquid region and

$$f''' + ff'' + \tfrac{1}{2}(1 - f'^2) = 0 \tag{3-8}$$

$$\phi'' + Pr\ f\theta' = 0 \tag{3-9}$$

$$\omega'' + Sc\ f\omega' = 0 \tag{3-10}$$

for the steam-hydrogen film. The appropriate normalized boundary conditions are (see Ref. [9])

$$\eta = 0: \quad f(0) = \frac{Y_i \omega'(0)}{Sc}\left(1 - \frac{M_I}{M_o}\right) \quad , \quad f'(0) = \theta(0) = \omega(0) = 0 \tag{3-11}$$

at the reaction front,

$$\eta = \eta_\delta: \begin{cases} F(0) = \epsilon\beta f(\eta_\delta) \quad , \quad F'(0) = \frac{1}{\epsilon} f'(\eta_\delta) \\ \qquad\qquad f''(0) = \beta f''(\eta_\delta) & (3\text{-}12) \\ \phi(0) = 0 \quad , \quad \theta(\eta_\delta) = 1.0 \quad , \quad \omega(\eta_\delta) = 1.0 & (3\text{-}13) \\ Y_i = \left[1 + \frac{\omega'(\eta_\delta)}{Scf(\eta_\delta)}\right]^{-1} & (3\text{-}14) \\ A\theta'(\eta_\delta) + Q_{rad} = f(\eta_\delta) + B\phi'(0) & (3\text{-}15) \end{cases}$$

at the steam film/liquid interface, and

$$\xi \to \infty: \quad F'(\xi) \to 1.0 \quad , \quad \phi(\xi) \to 1.0 \tag{3-16}$$

in the liquid far from the metal surface. In the boundary conditions, Eqs. (3-12) and (3-15), ϵ, β, A, B, and Q_{rad} are dimensionless parameters defined as

$$\epsilon = \left(\frac{\rho}{\rho_\ell}\right)^{1/2} \quad , \quad \beta = \left[\left(\frac{\rho}{\rho_\ell}\right)^{1/2} \frac{\nu}{\nu_\ell}\right]^{1/2} \quad , \quad Q_{rad} = \frac{\dot{q}_{rad}}{(2a/\nu)^{1/2} h_{fg} \nu\rho} \tag{3-17}$$

$$A = \frac{c(T_m - T_i)}{Pr\ h_{fg}} \quad , \quad B = \beta \frac{k_\ell}{k} \frac{c(T_i - T_\infty)}{Pr\ h_{fg}} \tag{3-18}$$

It should be noted that in Eqs. (3-17) and (3-18) the liquid/steam film interface temperature T_i is one of the unknowns of the problem. The steam mass fraction at the interface, Y_i, is related to T_i by virtue of the fact that the interface is a saturation state for the steam. The relationship is

$$\frac{P_{eq}(T_i)}{P_\infty} = \left[1 + \frac{M_o}{M_I}\left(\frac{1}{Y_i} \quad 1\right)\right]^{-1} \tag{3-19}$$

The two quantities of major interest are the outward convective heat flux $\dot{q}$ and the inward steam mass flux $\dot{m}_o$ at the reaction front. The former quantity is given by Fourier's law, $q = -k(\partial t/\partial z)_{t=0}$, while the latter quantity is given by Fick's law, $\dot{m}_o = -\rho D(\partial Y/\partial z)_{z=0}$. In terms of the transformed variables of Eqs. (3-3) and (3-5) the expressions for $\dot{q}$ and $\dot{m}_o$ become

$$\dot{q} = \frac{k(T_m - T_i)}{\beta} \cdot \frac{(6\ R_e)^{1/2}}{2R} \cdot \theta'(0) \tag{3-20}$$

$$\dot{m}_o = \frac{\rho D\ Y_i}{\beta} \cdot \frac{(6\ R_e)^{1/2}}{2R} \cdot \omega'(0) \tag{3-21}$$

During the course of this study several time-consuming attempts were made at finding a simplified approach to the solution of the set of equations given by Eqs. (3-6) through (3-19). These attempts included the application of the integral-profile (or Pohlhausen) method [27], a perturbation technique first proposed by Epstein and Hauser [24] for film boiling problems, and correlation of the numerical solutions of Eqs. (3-8) through (3-10) by various rational interpolation formulas. Unfortunately, none of these methods prove to be a satisfactory substitute for the complete numerical solution of Eqs. (3-6) through (3-19). The numerical method is described in Section 3.3. Values of the physical properties actually used in the computations are given in the next subsection.

3.2 Physical Properties

When a constant property analysis is applied to real fluids and fluid mixtures, it is common to take account of the temperature- and composition-dependence of the properties by employing reference temperatures and/or reference steam mass fractions. For the two regions under consideration here, the reference temperature and mass fraction for the hydrogen/steam film are

$$T_r = T_i + \gamma(T_m - T_i) \tag{3-22}$$

$$Y_r = Y_i(1 - \gamma)$$

while the reference temperature for the liquid (water) boundary layer is taken to be the film temperature

$$T_{\ell,r} = 1/2(T_i + T_\infty) \tag{3-23}$$

For most of the numerical calculations the constant γ was held fixed at the "film value" $\gamma = 0.5$. Some insight into the roles of the steam film reference temperature and reference composition was obtained by letting $\gamma = 0.3, 0.4$ for a few numerical cases.

The thermal conductivity and viscosity of the steam were taken from the tabulations of Ref. [21], to which the following curves were fitted:

$$\mu_{H_2O} = 1.57 \times 10^{-8}\ T_r^{1.126}\ , \quad \frac{kg}{m \cdot s} \tag{3-24}$$

$$k_{H_2O} = 4.47 \times 10^{-6}\ T_r^{1.447}\ , \quad \frac{W}{m \cdot K} \tag{3-25}$$

The corresponding properties of hydrogen were also obtained by curve fitting the tabular data of Ref. [21]. The results are

$$\mu_{H_2} = 1.99 \times 10^{-7}\ T_r^{0.669}\ , \quad \frac{kg}{m \cdot s} \tag{3-26}$$

$$k_{H_2} = 0.1175 + 3.15 \times 10^{-4}\ T_r\ , \quad \frac{W}{m \cdot K} \tag{3-27}$$

The thermal conductivity and viscosity of the steam/hydrogen gas mixture were evaluated from algebraic expressions based on the Lindsay-Bromley and Wilke mixture rules, respectively, for mixtures of polar and non-polar molecules. These mixture rules are presented and reviewed in Ref. [28]. The density of the steam/hydrogen film is given by the ideal gas law

$$\rho = \frac{M_{mix} P_\infty}{\bar{R}\, T_r} \tag{3-28}$$

where M_{mix} is the mixture molecular weight:

$$M_{mix} = [Y_r/M_o + (1 - Y_r)/M_I]^{-1} \tag{3-29}$$

Over the temperature range of interest (300 - 2000K), it is permissible to assume constant specific heats for the gas mixture components. The following values were used

$$c_{p,H_2O} = 2.2 \times 10^3 \ , \ \frac{J}{kg \cdot K} \ , \ c_{p,H_2} = 1.5 \times 10^4 \ , \ \frac{J}{kg \cdot K} \tag{3-30}$$

The mixture specific heat is calculated with the mixing rule

$$c_p = Y_r c_{p,H_2O} + (1 - Y_r) c_{p,H_2} \tag{3-31}$$

The computation of the coefficient of mass diffusion D for the steam/hydrogen mixture was carried out by the method outlined in Ref. [28] for polar-nonpolar gas pairs. The numerical results are well-represented by the expression

$$DP_\infty = 6.61 \times 10^{-4}\, T_r^{1.68} \ , \ \frac{m^2 \cdot Pa}{s} \tag{3-32}$$

The liquid (water) viscosity, thermal conductivity, and latent heat of evaporation were computed according to the expressions of Ref. [17]. These are

$$\mu_\ell = 10^{-3} \cdot \exp\left[-34.0294 + \frac{3046.63}{T_{\ell,r}} + 4.154 \ln(T_{\ell,r})\right] \ , \ \frac{kg}{m \cdot s} \tag{3-33}$$

$$k_\ell = 418.5(-7.925 \times 10^{-4} + 1.191 \times 10^{-5}\, T_{\ell,r} - 1.4542 \times 10^{-8} T_{\ell,r}^2) \ , \ \frac{W}{m \cdot K} \tag{3-34}$$

$$h_{fg} = 3.198 \times 10^{6}\left[1 - \left(\frac{T_i}{T_c}\right)\right]^{\left[0.6964 - 0.7797(T_i/T_c) + 0.4768(T_i/T_c)^2\right]}, \frac{J}{kg} \quad (3\text{-}35)$$

where T_c is the critical temperature of water (T_c = 647.29K). The liquid density was taken to be constant and given by $\rho_\ell = 10^3$ kg m^{-3}. Finally, the equilibrium vapor pressure of water that appears in Eq. (3-19) is given by the Clausius-Clapeyron form

$$P_{eq}(T_i) = 6.448 \times 10^{10}\exp\left(-\frac{4993.33}{T_i}\right), \quad Pa \quad (3\text{-}36)$$

Equation (3-36) is actually used in inverted form in Eq. (3-19), where for a given interfacial steam mass fraction Y_i we wish to determine the corresponding interface temperature T_i. For a given vapor pressure, Eq. (3-36) gives the corresponding absolute temperature to an accuracy better than about 4.0 percent for pressures from 2×10^3 Pa up to the critical pressure of 2.2×10^7 Pa.

3.3 Numerical Method

In order to obtain the steam mass flux $\dot{m}_o$ and the convective heat flux $\dot{q}$ to and from the reaction front, respectively, for given conditions T_∞, T_m, P_∞, R, and V_∞, the following steps were followed.

(1) A dimensionless film thickness $\eta_\delta = (2a/\nu)^{1/2}\delta$ was selected. A guess was made for the dimensionless suction velocity f(0) at the reaction front (or metal surface) and the vapor mass fraction Y_i at the steam film/liquid interface.

(2) The interface temperature T_i was then calculated from Eqs. (3-19) and (3-36). Using Y_i and T_i all the pertinent physical properties were calculated from the correlations given above in Section 3.2.

(3) A guess was made for the dimensionless shear stress at the reaction front (or metal surface) $f''(0)$. This value together with the guess for $f(0)$ [in Step (1)] and the boundary condition $f'(0) = 0$ [see Eq. (3-11)] provide three initial conditions for the steam/hydrogen film momentum equations. With these conditions, Eq. (3-8) was integrated in the positive η-direction to the location of the steam-liquid interface $\eta = \eta_\delta$. The values of f, f', and f'' at this location were transformed by matching conditions (3-12) into values $F(0)$, $F'(0)$, and $F''(0)$ which allowed integration of Eq. (3-6) into the liquid region. It was then necessary to check whether $F'(\xi)$ approaches the asymptote $F' = 1.0$ at large ξ [see boundary condition (3-16)]. If not, a new guess was made for the dimensionless shear stress at the metal surface $f''(0)$, holding both η_δ and $f(0)$ constant, and the entire integration was repeated until the condition $F'(\infty)$ was fulfilled. Once the correct value for $f''(0)$ was found, the solutions $f(\eta)$ and $F(\xi)$ were used as input data for the solution of the energy and diffusion equations (3-7), (3-9), and (3-10). The solutions of the differential equations provided the quantities $\theta'(0)$, $\theta'(\eta_\delta)$, $f(\eta_\delta)$, $\phi'(0)$, $\omega'(0)$, and $\omega'(\eta_\delta)$. The value of Y_i was obtained from Eq. (3-14).

(4) The values of Y_i and $\omega'(0)$ were then substituted into the first boundary condition of Eq. (3-11) to see if we recovered the assumed value of the suction velocity from Step (1). If not, a new value of $f(0)$ was chosen and Steps (2) through (4) were repeated until Eq. (3-11) was satisfied for the prescribed value of η_δ.

(5) The final equation that remains to be satisfied is the energy conservation condition at the steam/water interface, Eq. (3-15). If the values $\theta'(0)$, $f(\eta_\delta)$, and $\phi'(0)$ obtained

at end of Step (4) satisfied Eq. (3-15), the desired solution was found. Otherwise a new value of η_δ was chosen and Steps (2) through (5) were repeated.

Numerical integration of Eqs. (3-6) through (3-10) was performed using a forward integration procedure based on the Gear [29] method (see also Hindmarsh [30]). It should be noted that the present numerical solution of the two-phase stagnation flow problem represents an improvement over the technique reported by Epstein et al. [9]. In the previous work tables of $\theta'(0)$, $\theta'(\eta_\delta)$, etc. as functions of η_δ and f(0) were constructed from the numerical integrations of Eqs. (3-6) through (3-10). The tables were used in combination with Eqs. (3-11) and (3-15) to yield the solution. The tables were based on a priori estimates of the dimensionless groups Pr, Pr_ℓ, Sc, β, and ϵ that were not necessarily consistent with the final, solution values of Y_i and T_i. In the present numerical scheme, the physical properties of the product gas/vapor film and the liquid boundary layer are corrected during each iteration so that the appropriate correspondence between the final physical properties and the reference temperatures and concentration is achieved.

3.4 Transition from Vapor Phase to Surface Burning in Underwater Aluminum Oxidation

As mentioned previously, a change in reaction regime from vapor phase to surface burning is anticipated when the convective/diffusive supply of steam $\dot{m}_o$ cannot be consumed at the reaction front by the maximum possible rate of metal vapor supply, $\dot{m}_{vac}$. Based on the work of Turkdogan et al. [14] we anticipate that when the vacuum vaporization rate of the metal becomes comparable to the incoming steam transport rate the reaction front moves to within a few gas mean-free-paths of the metal surface, as illustrated in Fig. 3-1. Thus by combining the criterion (2-3) with the theory given in the foregoing for $\dot{m}_o$ for steam transport to a hot metal surface immersed in water in film boiling we can identify the metal temperature level required to support vapor phase burning under water.

The critical metal temperature is found by solving the equation given by [see Eqs. (2-1), (2-3), and (3-21)]

$$\dot{m}_{vac}(T_m) = \frac{P_{eq,m}(T_m)}{(2\pi \bar{R} T_m/M_m)^{1/2}} = \frac{M_m \rho D Y_i}{M_o n \beta} \cdot \frac{(6 R_e)^{1/2}}{2R} \cdot \omega'(0) = \frac{M_m}{M_o n} \left| \dot{m}_o(T_m) \right| \tag{3-37}$$

The numerical solutions for Y_i and $\omega'(0)$ indicate that these quantities are somewhat sensitive to the metal temperature T_m. Thus the solution for the critical T_m is best done by plotting the functions $\dot{m}_{vac}(T_m)$ and $\dot{m}_v(T_m)$ and seeking their intersection, at which Eq. (3-37) is satisfied identically.

3.5 Gas-Phase Transport-Limited Oxidation Heating of Aluminum Spheres Under Steam Explosion Conditions

As will be seen later on, it is very unlikely that vapor phase burning is the mechanism of aluminum oxidation during a steam explosion. Thus it becomes necessary to show that a surface reaction model is capable of accounting for the events following the onset of a physical vapor explosion that takes us from a melt of pure aluminum to microspheres of nearly stoichiometric Al_2O_3. A complete understanding of how this occurs requires a theory that explains the ineffectiveness of the normally very protective oxide layer during the roughly millisecond time scale of the steam explosion. This is a formidable task that has not been considered as part of the present effort but certainly provides ample opportunities for further theoretical work. At the present time all we can do is assume that the protective oxide does not form or is swept away by the steam explosion "forces" and, therefore, hope that aluminum combustion during a steam explosion may be profitably regarded as a surface burning phenomena that is limited by steam diffusion and convection within the gaseous steam/hydrogen film that envelope the droplets (microspheres) that comprise the fine fragmented aluminum melt produced during the course of the steam explosion. Using this approach, which was used previously by Young and Nelson [8], we can search for conditions under which an aluminum droplet will quench rather

than heatup, and we can see if the "film-side" steam transport rate is compatible with the oxidation time scale required to liberate chemical energy during a steam explosion.

During an explosion a representative molten aluminum sphere moves relative to the surrounding liquid and its surface temperature is continually changing with time. Thus thermal convection in the liquid and heat and mass transport in the steam film should be unsteady. However, it can be shown that the time necessary for a diffusion wave to span the film dimension δ or the liquid boundary layer thickness is much smaller than the sphere oxidation time. Thus the rate of steam flow to the sphere should quickly approach a quasi-steady value given by the solution of the conservation equations presented in Section 3.1. The essential features of this quasi-steady oxidation process can be obtained from a study of two conservation equations that must be solved simultaneously with the steady-state theory of Section 3.1 - namely, an energy balance and an oxidizer (steam) balance. The first, required because the aluminum sphere temperature governs the rate of evaporation of steam, equates the sum of energy losses (convection and radiation through the steam/hydrogen film, and sphere enthalpy change) to the energy source due to the steam-metal surface reaction; the second restates the fact that the kinetic rate of steam incorporation at the surface must equal that supplied by diffusion and convection from the external steam/hydrogen film.

A simplified energy balance may be written by (1) ignoring heat conduction limitations within the aluminum sphere and (2) assuming that most of the heat and mass is transferred to the front half of the moving sphere at rates determined from the solution of the governing equations for stagnation flow. The latter assumption follows from the arguments advanced in Refs. [9,24] that convective mass and heat transfer are negligible on the downstream side of the reacting sphere where the vapor film is transformed into a thick vapor wake. Of course heat is radiated outward from the entire surface of the sphere. If τ denotes time then the rate of rise of sphere temperature is given by

$$\frac{4}{3}\pi R^3 \rho_m c_m \frac{dT_m}{d\tau} = 2\pi R^2 \cdot \frac{\dot{m}_o \Delta H}{nM_o} - 2\pi R^2 \dot{q} - 4\pi R^2 \dot{q}_{rad} \qquad (3\text{-}38)$$

where the remaining quantities are defined in the Nomenclature. A value of $\Delta H = 4.96 \times 10^8$ J (kg-mole)$^{-1}$ of metal reacted is taken as the heat of reaction. Note that $\dot{q}$ and $\dot{m}_o$ in the above equation are given by Eqs. (3-20) and (3-21), respectively.

The net rate of steam uptake by the metal sphere is simply $4\pi R^2 \dot{m}_o$. From stoichiometry, the rate of metal being reacted is $4\pi R^2 \dot{m}_o M_m/(nM_o)$. If F_m represents the mass fraction of metal reacted, the net rate of metal oxidized is

$$\frac{4}{3}\pi R^3 \rho_m \frac{dF_m}{d\tau} = 4\pi R^2 \frac{\dot{m}_o M_m}{nM_o} \qquad (3\text{-}39)$$

Again, this equation is based on the notion of oxidation limited by "steam-film-side" properties. No consideration has been made of internal transport or chemical limitations to aluminum sphere oxidation. A discussion of limitations internal to the sphere is postponed until later on.

An elementary Euler method was used to solve Eqs. (3-38) and (3-39) for the sphere temperature and reaction histories $T_m(\tau)$ and $F_m(\tau)$, given the initial values $T_m(0)$ and $F_m(0) = 0$. At each time step T_m is known and the boundary conditions in the liquid far from the sphere, T_∞, P_∞, and V_∞ are given. Thus the variable T_m may be regarded as just another boundary condition for the steady-state two-phase film-boiling boundary-layer analysis, and at each time step equations (3-6) through (3-16) were solved to yield the fluxes $\theta'(0)$ and $\omega'(0)$ and the steam concentration and temperature at the liquid/steam interface, Y_i, T_i. The procedure for obtaining $\theta'(0)$, $\omega'(0)$, Y_i and T_i has already been outlined in Section 3.3.

4.0 RESULTS AND DISCUSSION

Representative steam mass fraction and temperature profiles and convective heat and mass fluxes for the steady-state stagnation flow of water over a hot aluminum sphere are to be presented first. These figures will provide a feeling for (1) the accuracy of previous theoretical work in the area of metal-water reactions and (2) the importance of thermal radiation to the reacting sphere overall heat balance. This will be followed by a presentation of the predicted critical metal temperatures for the transition from vapor phase to surface burning under quiescent and steam explosion conditions. Finally, quantitative estimates of the time scale for complete oxidation of aluminum microspheres are compared with measured aluminum-water explosion time scales. The implications of these theoretical results in terms of the potential for producing ignition type steam explosions are discussed.

4.1 Structure of Steam-Hydrogen Film in the Stagnation Region of an Isothermal Sphere Oxidizing at a Rate Limited by Steam Transport

Figure 4-1 shows the temperature and steam mass fraction profiles for a 1.0-cm diameter reactive aluminum sphere freely falling through water at a velocity $V_\infty = 0.64\ m\ s^{-1}$. It should be mentioned that the terminal velocity of the sphere is calculated from the following momentum balance between sphere drag and buoyancy:

$$C_D R_e^2 = \frac{32R^3(\rho_m/\rho_\ell - 1)g}{3\,\nu_\ell^2} \tag{4-1}$$

where C_D is the drag coefficient given by the empirical expression [31]

$$C_D = \begin{cases} \frac{24}{Re}\left(1 + 0.15\ Re^{0.687}\right) & Re < 10^3 \\ 0.44 & Re \geq 10^3 \end{cases} \tag{4-2}$$

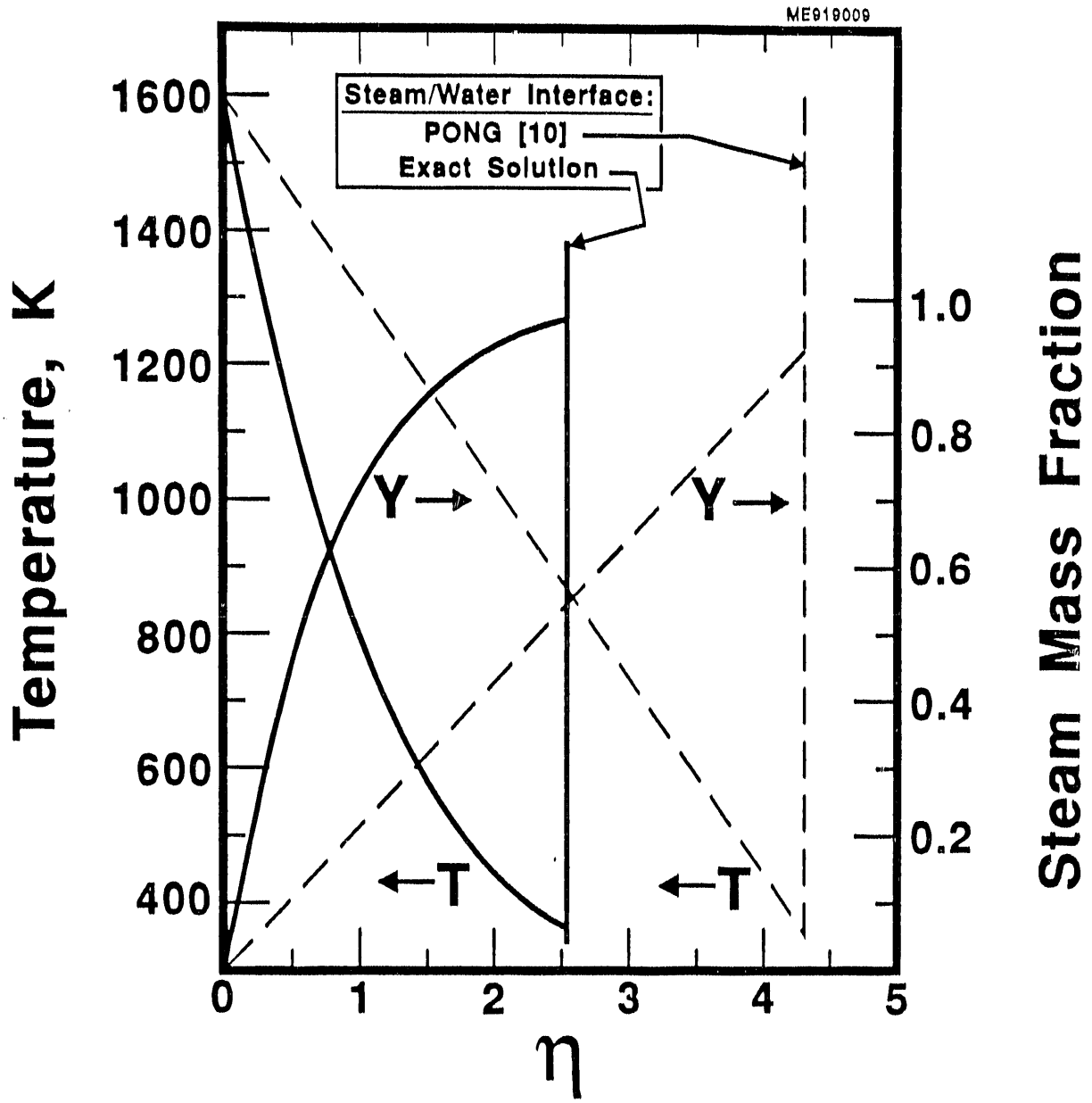

Figure 4-1 Representative temperature and steam mass fraction profiles in steam/hydrogen film, comparison of exact (numerical) solution (solid curves) with Pong's analysis (dashed curves). Conditions: $T_m = 1600K$, $T_\infty = 373K$, $R = 5 \times 10^{-3}$ m, $V_\infty = 0.64$ $m^m s^{-1}$, $P_\infty = 10^5$ Pa, $\gamma = 0.5$, $e = 1.0$.

Once the Reynolds number Re is determined from the solution of the above equations, the sphere velocity follows from the definition of Re:

$$V_\infty = \frac{\nu_\ell Re}{2R} \tag{4-3}$$

Actually the numerical solution of Eqs. (4-1) and (4-2) was carried out as part of the solution procedure for the film-boiling boundary-layer equations described in Section 3.3. Thus the predicted value of V_∞ is based on the physical property values (particularly ν_ℓ) used in the boundary layer solution. The remaining conditions appropriate to Fig. 4-1 are: metal temperature T_m = 1600K, molten metal density ρ_m = 2360 kg m^{-3}, system pressure $P_\infty = 10^5$ Pa, saturated water T_∞ = 373K, and radiative emittance e = 1.0.

It may be seen from Fig. 4-1 that the temperature and mass fraction profiles in the film are not straight, indicating that convection, reaction-induced suction, and evaporation (blowing) play a large role in the transport of heat and mass. These effects have been largely ignored in the metal-water reaction theory reported by Pong [10]. She set aside the nonlinear inertia and mass and energy convection terms in the boundary layer equations for the steam/hydrogen film, essentially following an earlier perturbation approach to film boiling on inert, hot surfaces by Epstein and Hauser [24]. Some care must be exercised, however, in neglecting the effects of vapor film inertia and convection as these effects become significant at high surface temperatures. Epstein and Hauser were interested in film boiling applications in which the temperature of the hot surface was less than about 800K. In this relatively low-temperature regime the neglect of the nonlinear terms in the boundary layer equations is permissible. It is obvious from Fig. 4-1 that the nonlinear terms are crucial for the high surface temperatures encountered during aluminum-water reactions.

Figures 4-2 and 4-3 compare the present theoretical results for the steam mass flux $\dot{m}_o$ and the convective heat flux $\dot{q}$ at the reactive surface

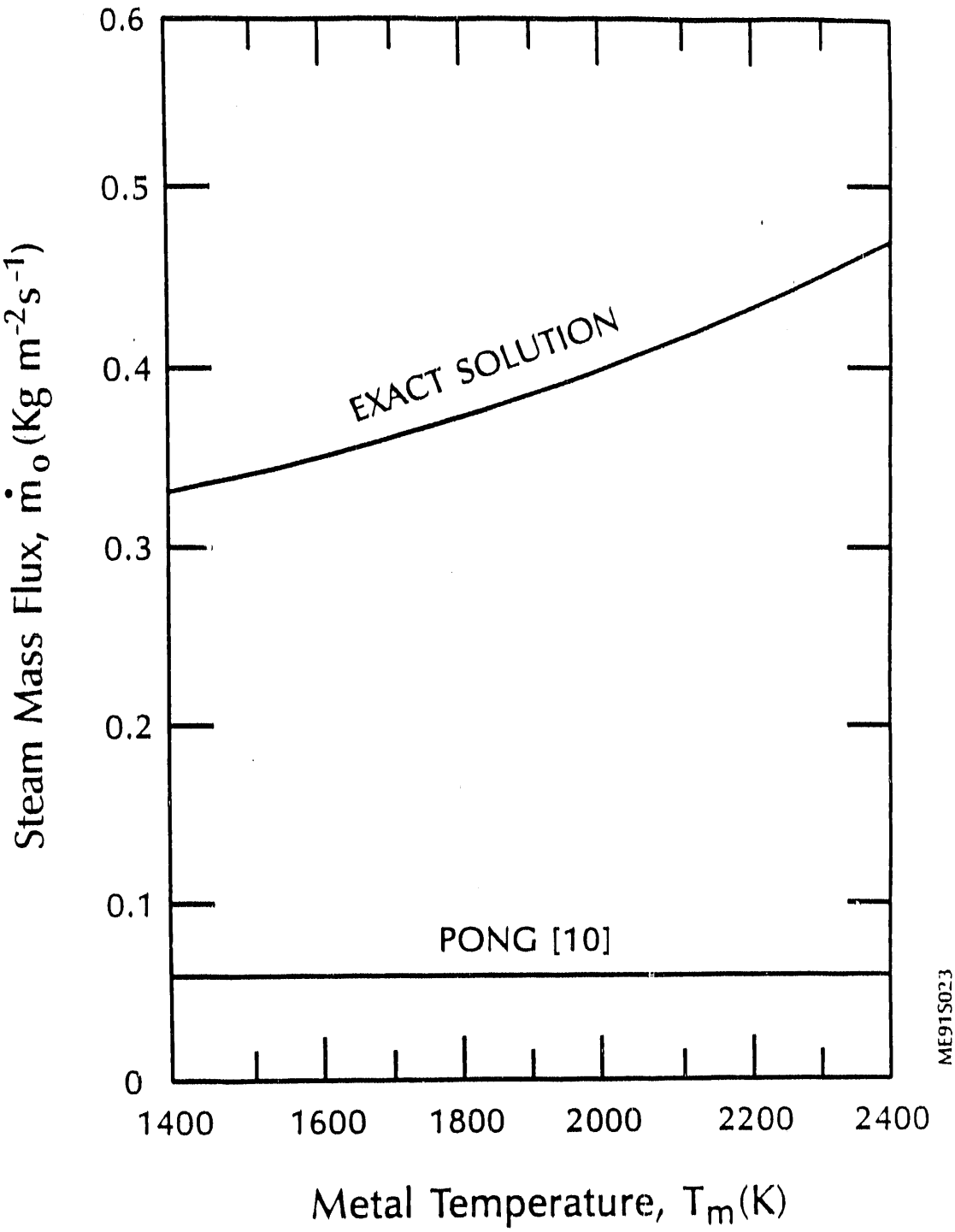

Figure 4-2 Representative steam mass flux to reactive metal sphere as a function of sphere temperature, comparison of exact (numerical) solution with Pong's analysis. Conditions: T_∞ = 373K, R = 5 x 10^{-3} m, V_∞ = 0.64 m s^{-1}, P_∞ = 10^5 Pa, e = 1.0, Y = 0.5.

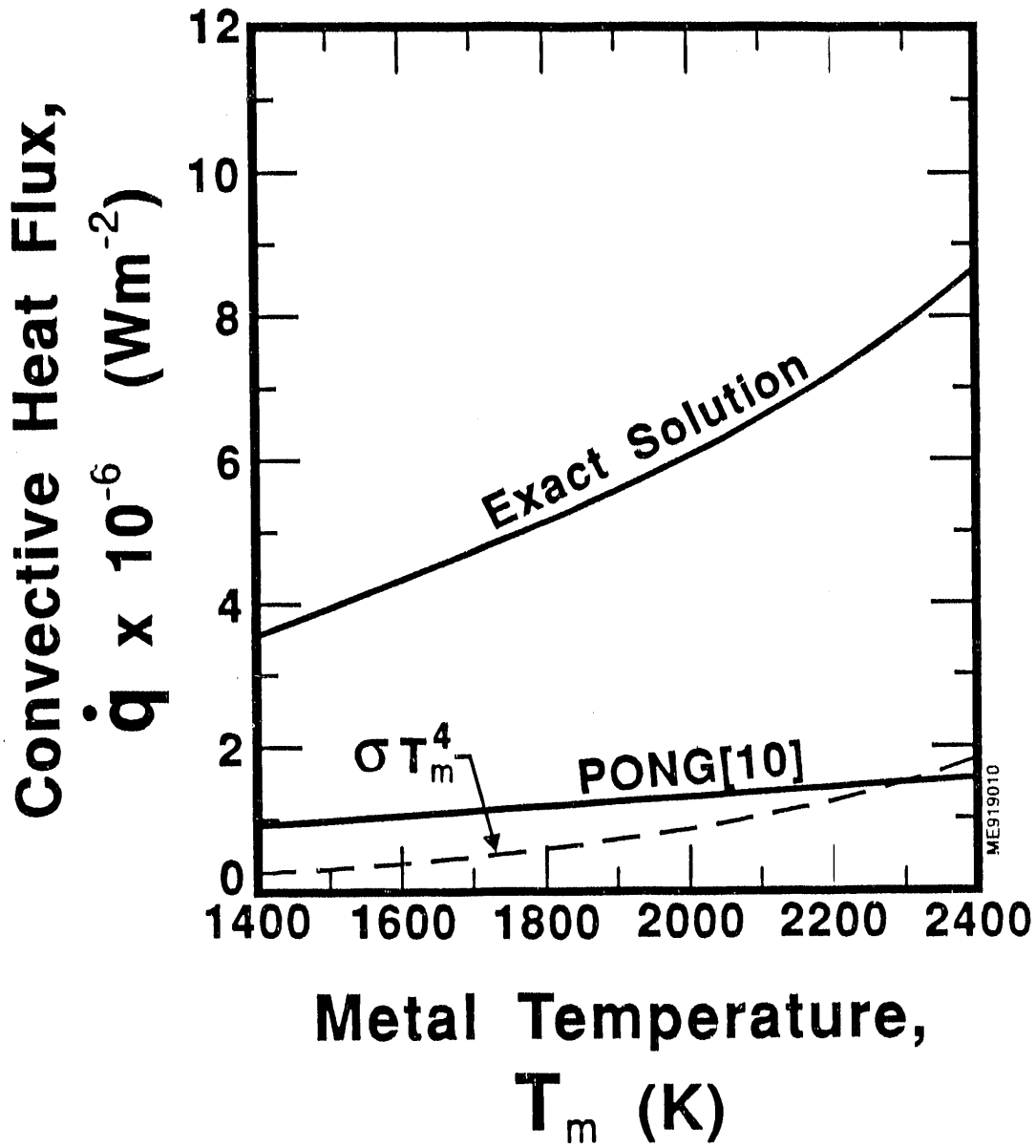

Figure 4-3 Representative convective heat flux from reactive metal sphere as a function of sphere temperature, comparison of exact (numerical) solution with Pong's analysis. Conditions: T_∞ = 373K, R = 5 x 10^{-3} m, V_∞ = 0.64 m s^{-1}, P_∞ = 10^5 Pa, e = 1.0, γ = 0.5.

with the theory of Pong [10] for a range of metal surface temperatures. The curves were constructed for a 1.0-cm diameter aluminum sphere falling through saturated water at $P_\infty = 10^5$ Pa. As a result of neglecting profile distortions, Pong's model underestimates the values of $\dot{m}_o$ and $\dot{q}$ by more than a factor of five. Pong's model has been used by Young and Nelson [8] in their theoretical study of the underwater oxidation of aluminum drops. They predicted a metal temperature threshold of 1100K for aluminum ignition under water. Above 1100K the oxidation heating rate, limited by film-side steam transport exceeded the heat loss rate from the aluminum sphere due to convection and radiation. Below 1100K the chemical heating rate was predicted to be less than the heat loss rate and the sphere cooled. Considering the inaccuracies inherent in Pong's model, Young and Nelson's finding of a temperature threshold controlled by steam-film heat and mass transport should be regarded with caution (see Section 4.4).

An interesting feature of Fig. 4-3 is that radiation is negligible compared with convection, even at metal temperatures as high as 2400K. Thus thermal (or runaway) theories of underwater aluminum ignition, such as that of Kuan and Buescher [6], which only consider radiation heat losses produce results which are not very accurate.

4.2 Minimum (Critical) Metal Temperature for Vapor Phase Burning Under Quiescent Conditions

To illustrate the use and behavior of Eq. (3-37) for the minimum metal temperature at which vapor phase burning is possible we have carried out calculations for aluminum spheres in free-fall in water and for a representative aluminum sphere in a fragmented melt-water mixture in the wake of a pressure shock. The computational results for the latter situation, which is believed to be applicable to the propagation phase of a steam explosion, are presented in the next subsection.

Figure 4-4 is constructed for pure aluminum spheres and for spheres of aluminum alloys 6061 and 6063 in free-fall in water at atmospheric pressure.

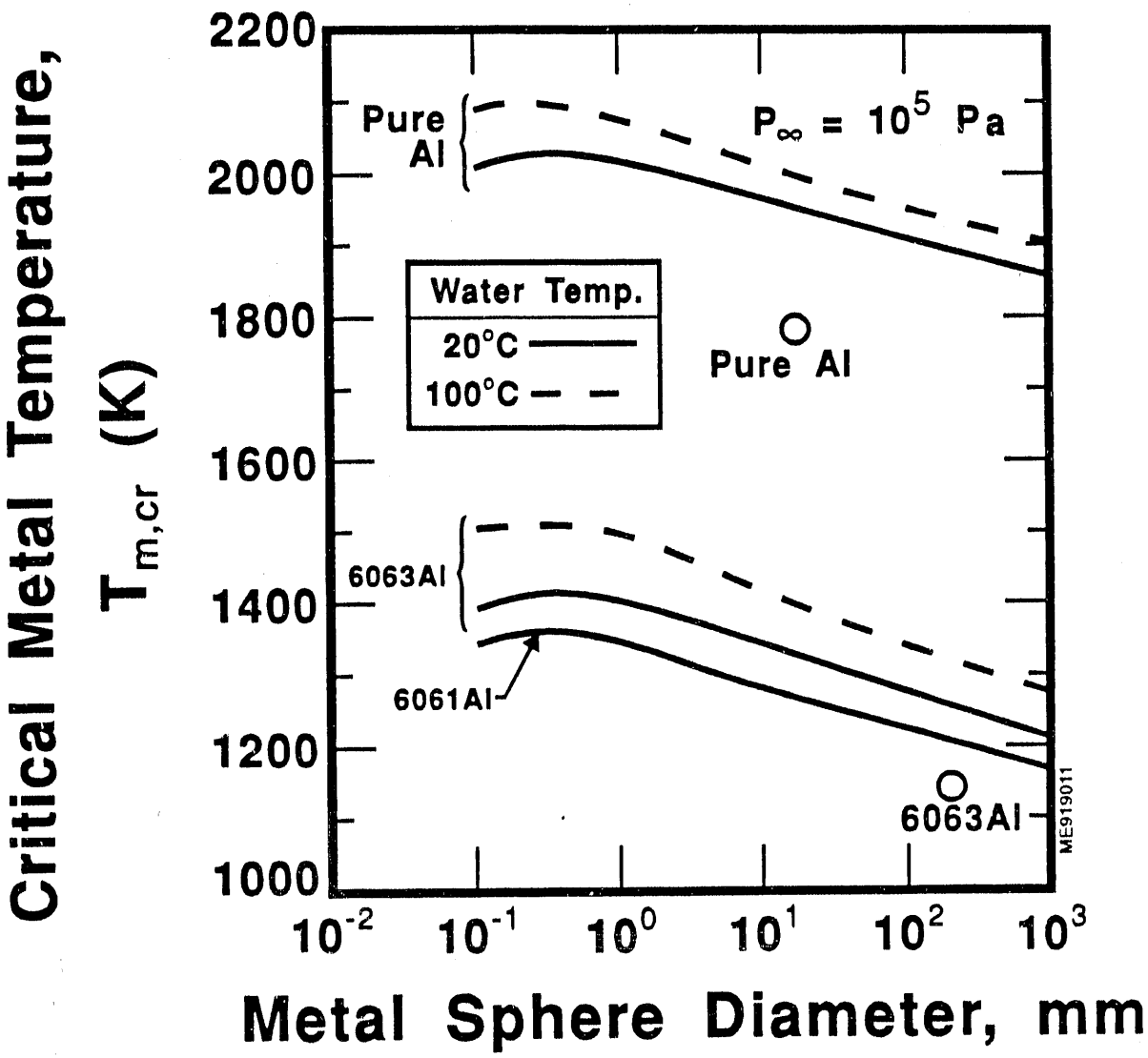

Figure 4-4 Effects of sphere diameter and water temperature on the critical (minimum) metal temperature for vapor phase burning of aluminum spheres in free fall in water. The circles pertain to observed threshold metal temperatures for ignition-type steam explosions with pure Al and 6063 Al in room temperature water [5,4].

We note that the substitution of subcooled water for saturated water produces a modest decrease in the critical temperature for vapor phase burning. The steam flux to the reactive surface under saturated boiling conditions is greater than that under subcooled boiling conditions. Thus the minimum metal surface temperature $T_{m,cr}$ required in order for the metal vaporization rate to be capable of matching the supply rate of steam from saturated water is higher than the $T_{m,cr}$ required when steam is produced from subcooled water. Also, the larger the size of the reactive sphere the poorer is the conditions for steam transport to the reactive surface. Thus for a given metal temperature level large reactive spheres can more readily prevent steam from reaching their surfaces than smaller reactive spheres. However, as can be seen from Fig. 4-4, the critical temperature versus sphere diameter trend reverses direction when the sphere diameter falls below about 1.0 mm. This is because the decrease in steam mass transport rate due to decreasing sphere terminal velocity more than makes up for the increase in steam transport rate as the sphere size is decreased into the sub-millimeter range.

The effect of changing the sphere material from pure aluminum to either 6061- or 6063-aluminum alloy is very large. This is due to the fact that these alloys contain small quantities of magnesium, which is a much more volatile substance than aluminum. The lower theoretical $T_{m,cr}$ versus sphere diameter curves in Fig. 4-4 were obtained by assuming that the magnesium-aluminum mixture is ideal and employing the magnesium equilibrium vapor pressure expression (taken from Ref. [19])

$$P_{eq,Mg} = \frac{8.22 \times 10^{14}}{T_m^{1.41}} \exp\left(-\frac{1.7385 \times 10^{5}}{T_m}\right) \qquad (4\text{-}4)$$

The product of the magnesium mole fraction (1.11×10^{-2} and 7.77×10^{-3} for 6061Al and 6063A, respectively) and $P_{eq,Mg}$ was substituted for $P_{eq,m}(T_m)$ in Eq. (3-37). In spite of the fact that magnesium is present in the alloys in trace quantities, its vapor pressure is high enough to support a vapor phase reaction zone at temperatures as low as 1200K. As pointed out by Baker and

Simms [11], several experimental studies have indicated that vapor phase burning between magnesium containing aluminum alloys in steam can occur at rather low temperatures (~ 1200K).

It is of interest to compare the critical temperature for vapor phase burning predicted according to the present film boiling model with the measured threshold temperatures for ignition-type steam explosions in the single drop tests by Nelson et al. [5] and in the large scale tests reported by Rightly and Beck [4]. In the small scale tests aluminum ignition was achieved with a roughly 10^{-2} kg melt drop of pure aluminum when the melt temperature exceeded 1773K. The large scale test program [4] revealed a temperature threshold of about 1150K below which chemical energy was not believed to be liberated. These tests were carried out with roughly 10 kg masses of 6063 aluminum alloy. The measured threshold temperatures are plotted in Fig. 4-4 as a function of the size of the metal spheres that would be attained if they had the same volume as the aluminum melt mass delivered to the water. The purpose of plotting the threshold temperatures in this manner is simply to emphasize the difference in aluminum melt scale between the small- and large-scale tests. Actually, upon entering the water, the melt in the large scale tests breaks up into particles of diameters of the order of those used in the small-scale tests.

In comparing the measured threshold ignition temperatures with the predicted minimum temperatures for vapor phase burning of spheres of aluminum or its alloys in free-fall through water we are, in a sense, proposing that vapor phase burning during the so-called fuel-coolant premixing configuration period is a necessary condition for the release of chemical energy during the subsequent steam explosion event. However, at this stage of our understanding several questions or concerns my be raised regarding the validity of this postulated ignition condition. While the comparison in Fig. 4-4 is encouraging the observed ignition thresholds lie about 150K below what is supposed to be the minimum possible metal temperatures that are capable of supporting a vapor phase reaction zone. More refined calculations that account for the increase in the metal surface

temperature during the transient period immediately following aluminum-water contact and the concomitant appearance of a flame front may reduce the discrepancy between measured and predicted temperature thresholds. In the large scale tests with aluminum alloys the quantity of magnesium is too small to raise the bulk metal temperature by more than approximately 200K, even if one assumes that all the heat of reaction is dissipated solely by raising the metal temperature. This introduces the following question: how can the rapid vapor phase burning mode be sustained before all the magnesium is consumed? Perhaps the early vapor phase burning of magnesium raises the surface temperature of the metal to some second-level threshold temperature at which rapid burning may proceed by a different mechanism. A switch to vapor phase burning of aluminum at a metal surface temperature of about 2000K is possible (see Fig. 4-4). Alternatively, it has been suggested that if the surface temperature can be raised to the aluminum oxide melting temperature of 2320K a rapid surface reaction may begin [8]. To examine the potential for rapid surface heating it will be necessary to predict the magnesium-steam reaction front temperature via an appropriate vapor phase burning model. More serious criticisms of the vapor-phase burning theory of ignition are (1) the absence of any "reported observations" by Nelson et al. [5] and Rightly and Beck [4] of vapor-phase diffusion flames during the period just prior to a recorded explosion when the aluminum melt is falling through water and (2) the pressure-shock initiated explosions reported by Lemmon [3] using "commercially pure" aluminum at the relatively low temperature of about 1300K. Lemmon does state, however, that sodium metal was present in the aluminum at a low but unknown concentration. Sodium metal is very volatile so that vapor phase oxidation is possible for small concentrations of this metal.

Thus, while the vapor phase burning mechanism offers a theoretical basis for aluminum ignition temperature thresholds during steam explosions, it is clear that further theoretical and experimental work is needed to confirm its validity or, perhaps, to identify a different ignition mechanism that is more compatible with the observations.

4.3 Minimum (Critical) Metal Temperature for Vapor Phase Burning Under Steam Explosion Conditions

Before we can apply the film boiling theory and Eq. (3-37) to predict the critical metal temperature for the conditions that prevail during a steam explosion, it is necessary to determine the characteristic size R of the fragmented aluminum melt spheres (drops) and the velocity V_∞ of the aluminum spheres relative to the surrounding coolant.

The best information available from high-speed photography of steam explosions in progress suggests that a reaction front or pressure shock propagates through an initial course mixture of metal melt and water. Behind the pressure shock, the characteristic size of the melt particles is reduced from centimeters to sub-millimeter size during a time period of roughly 1.0 msec. To avoid obscuring complications, and to obtain simple expressions for the liquid velocity V_∞ and for the particle radius R behind the shock we assume that the shock obeys the acoustic approximation. Thus the water velocity behind the shock is related to the shock strength P_∞ by the expression

$$V_\infty = \frac{P_\infty - P_a}{\rho_\ell \, c_s} \tag{4-5}$$

where P_a is the pressure of the ambient medium upstream of the shock and c_s is the sound speed in liquid water (1500 m s^{-1}). In writing Eq. (4-5) we have ignored the attenuation of the shock by the presence of the vapor phase or, for that matter, the possible reinforcement of the shock by the coalescence of the reaction zone and the acoustic (precursor) shock.

The sudden dynamic effect of the surrounding water motion V_∞ relative to the coarse metal drops behind the shock is a plausible mechanism for the subdivision of the metal into fine drops. The approach to metal-drop breakup followed here is identical to that proposed by Epstein and Fauske [32] in their analysis of the breakup of molten jets in water. Briefly, a capillary wave breakup mechanism is considered. When a capillary wave along

the surface of a course, premixture configuration drop has grown to a size comparable with its wavelength, the crust of the wave is eroded as a droplet whose diameter 2R is approximately determined by the length of the most unstable wave. This metal-drop breakup criterion, together with linear Kelvin-Helmholtz instability analysis, results in the following expression for the characteristic size of the fragmented metal material

$$R = \frac{3(\rho_m + \rho_\ell)(\sigma_m + \sigma_\ell)}{4\,\rho_m \rho_\ell\, V_\infty^2} \tag{4-6}$$

where σ_m and σ_ℓ are, respectively, the surface tensions of the molten metal and water materials ($\sigma_m + \sigma_\ell \approx 0.93$ N m^{-1}). For purposes of the present discussion it is significant to observe that the thickness of the steam film that surrounds the coarse premixture configuration drop is predicted to be negligible compared with the size of the eroded drops, as given by Eq. (4-6). Under these conditions the steam film does not seriously influence the metal breakup process [32].

The combination of Eqs. (4-5) and (4-6) defines the values V_∞ and R sought. Some selected results are shown in Table 4-1 for an ambient pressure $P_a = 10^5$ Pa. The predicted critical temperature for vapor phase burning of the fragmented particles behind the shock front as a function of shock pressure is shown in Fig. 4-5. The effect of increased water temperature is seen to give rise to the expected increase in the critical metal temperature. Along the dark curve (labeled saturated) in Fig. 4-5 the water temperature increases with increasing shock pressure P_∞; that is, the water behind the shock is assumed to be instantaneously heated to its saturation temperature at the pressure P_∞. It is clear from Fig. 4-5 that self-sustained aluminum metal oxidation in the vapor phase flame mode is virtually impossible for initial melt temperatures of practical interest. For example, based on Fig. 4-5 we estimate that the bare surfaces of the fragmented aluminum material behind a shock of strength $P_\infty = 5$ MPa are incapable of supporting a vapor phase reaction front at any temperature below 2450K. Thus, while the chemical energy release process may be started

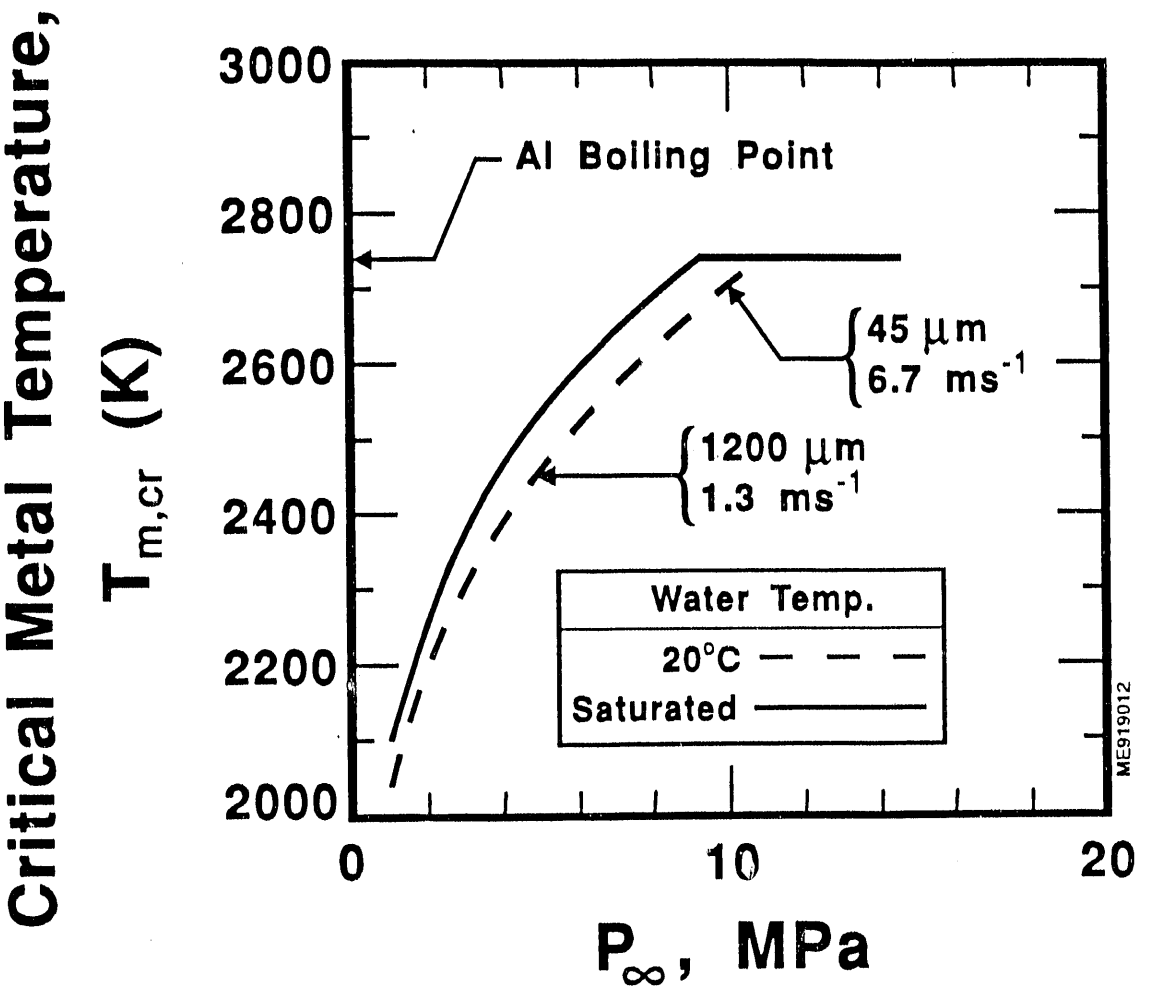

Figure 4-5 Effect of "trigger shock" pressure on the critical (minimum) water temperature for vapor phase burning of aluminum microspheres behind the shock. Liquid velocity and corresponding metal particle size indicated along curve for subcooled water.

in the vapor phase in the metal-water premixture, it must continue as a surface reaction once the explosion begins.

Table 4-1

PREDICTED WATER VELOCITY V_∞ AND ALUMINUM MICROSPHERE RADIUS R BEHIND "TRIGGER" SHOCK AS A FUNCTION OF SHOCK PRESSURE P_∞ (P_a = 0.1 MPa)

P_∞, MPa	V_∞, m s^{-1}	R, μm
1	0.67	2235
2	1.33	559
5	3.33	89.4
10	6.67	22.4
20	13.32	5.6

It is pertinent to note that the results presented in Fig. 4-5 are based on the assumption that the relative velocity between the reacting microsphere (particle) and the water coolant remains constant and equal to the initial value V_∞. We will see in the next subsection that time it takes for a representative aluminum particle to accelerate up to the liquid velocity is considerably less than the particle oxidation time so that this assumption of complete fluid "slip" may not be valid. Perhaps a heat- and mass-transport model for a stationary sphere with respect to the boiling coolant that accounts for V_∞ decreasing with time would be more appropriate for the purpose of estimating the critical temperature for vapor phase burning. It is doubtful, however, that this model would alter our conclusion regarding the impossibility of vapor phase burning under violent aluminum/water contacting conditions.

4.4 Steam-Phase Transport-Controlled Heatup of a Reacting Aluminum Sphere

In the past the ignition of several metals, e.g., zirconium, has been successfully explained by the application of thermal explosion theory. The application of a kinetic rate law for the surface reaction and an energy balance revealed a critical temperature above which metal-droplet self-heating occurs. There was no need to postulate exotic initiating mechanisms, such as vapor phase burning. Unfortunately, all the available direct measurements of aluminum oxidation (see Baker and Simms [11]), which were obtained under quiescent conditions, suggest that if steam reaches the metal surface an abrupt many-decade reduction in the aluminum oxidation rate occurs. An empirical kinetic expression that correlates the laboratory data on aluminum surface (internal) oxidation rates has been proposed by Baker and Simms [11]. Using this purely chemical-controlled reaction rate correlation, the energy balance Eq. (3-38) together with the film-boiling theory of Section 3.1 would merely state that the aluminum microspheres that suddenly appear in a steam explosion zone only experience cooling and release an insignificant fraction of their "stored" chemical energy, regardless of the initial temperature of the aluminum melt. On the other hand, it is possible for rapid chemical reaction to proceed beneath the surface of the aluminum if, during the extremely short time scale and under the prevailing high pressure of a steam explosion, incipiently formed condensed oxide is unstable with respect to the underlying aluminum melt. We can estimate the maximum possible surface oxidation rate in the absence of an oxide layer by assuming that the combustion is controlled by diffusion and convection of steam across the hydrogen/steam film.* However, with regard to developing an ignition model based on surface burning, further experimental and theoretical work must be done to determine the stability limits of the protective oxide surface skin. Here we present the predictions of the

---

*. In the calculation of the oxidation rate of a "bare" aluminum surface the distinction between surface burning and vapor-phase burning loses much of its significance, since in both cases the rate is limited by steam transport within the gaseous film.

steady-state boundary layer equations for the hydrogen/steam film and the water together with the unsteady energy and mass balance Eqs. (3-39) and (3-40).

Calculated temperature-time and percent reaction-time histories for an aluminum sphere for different steam-film physical property weighting factors γ are shown in Fig. 4-6. The calculations were carried out for an aluminum particle (sphere) in water, instantaneously heated to its saturation temperature T_∞ = 569K in the wake of a 10 MPa pressure shock (see Table 4-1). The initial temperature of the molten metal sphere was taken to be $T_m(0)$ = 1100K. Recall that these calculations are based on the assumption that the chemical reaction is controlled solely by gas-phase transport in the film enveloping the aluminum sphere. The transient energy balance reveals that initially heat is generated by oxidation at a greater rate than it is lost by convection and radiation. However, as the temperature of the sphere increases, the heat flux from the sphere increases at a greater rate than the steam flux to the surface and the oxidation heating rate and the heat loss rates tend to come into balance. Note that the sphere temperature versus time curves begin to level off when the right-hand-side of Eq. (3-39) approaches zero. Of course, the effective oxidation heating period suddenly terminates when the sphere is completely oxidized (F_m = 1.0). The stage of net particle cooling is not shown in Fig. 4-6. We note from Fig. 4-6 that the maximum temperature achieved by the sphere and the oxidation time are somewhat sensitive to the choice of γ, which determines the reference temperatures for steam-hydrogen-film physical property evaluations during the heatup transient.

The particle heatup curves shown in Fig. 4-6 are typical of most of the numerical cases considered in the present study. As mentioned previously, our numerical results do not support those of Young and Nelson [8] in that a low-metal temperature threshold that separates net particle heating from cooling was not observed in the present study. Our calculations do indicate a runaway threshold with respect to the water temperature T_∞. When T_∞ is reduced below about 50°C a net energy loss and droplet quench is predicted.

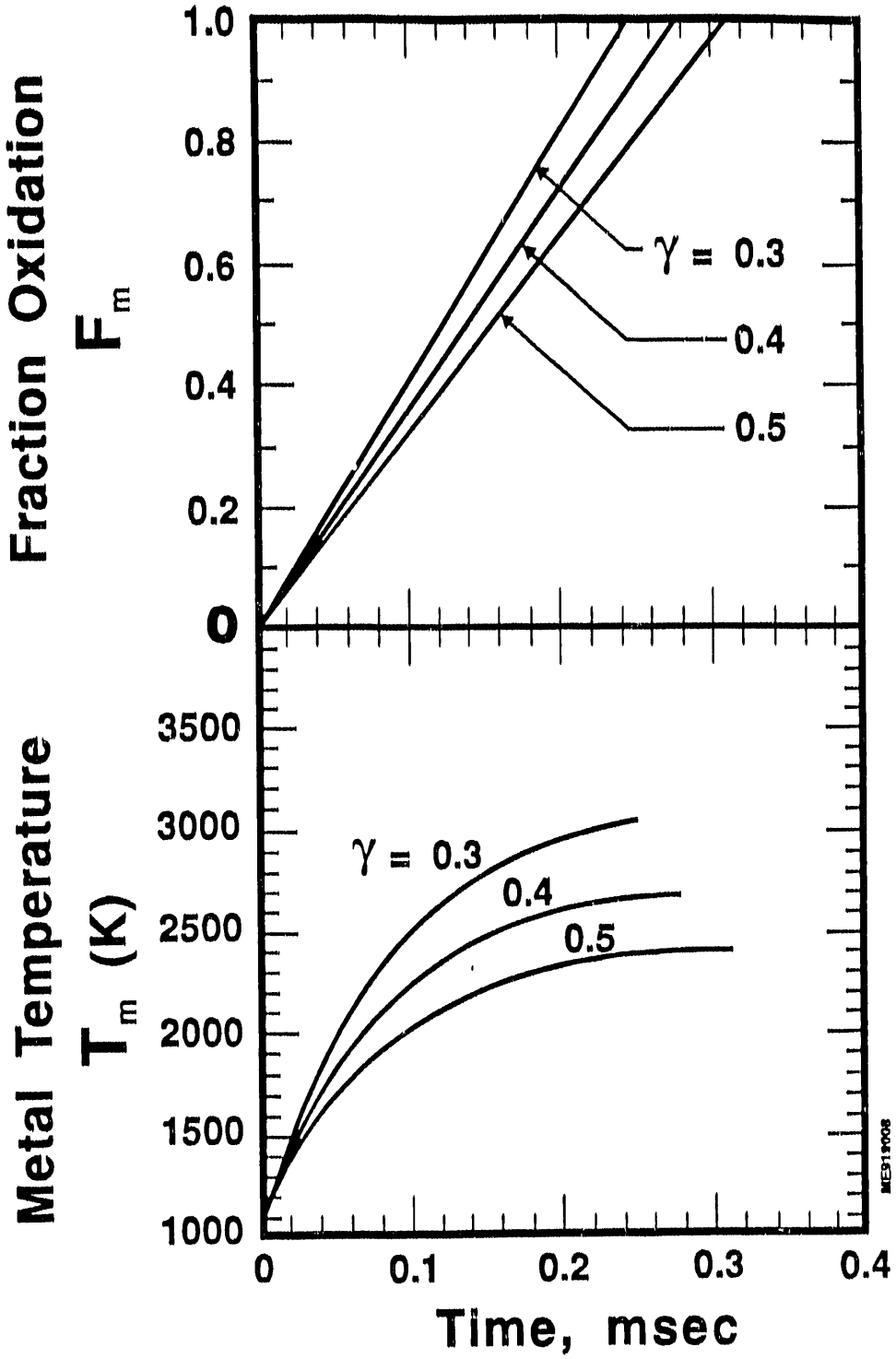

Figure 4-6 Effect of steam-hydrogen film physical property weighting factor γ on sphere oxidation and temperature time histories. Conditions P_∞ = 10 MPa, V_∞ = 6.67 m s^{-1}, R = 22.4 μm (see Table 4-1), $T_m(o)$ = 1100K.

However, this finding is not regarded as significant. On physical grounds, during the initial stages of the explosion, the water temperature must rise rapidly through 50°C on its way to a near saturated state. A threshold metal temperature is possible only when the right-hand-side of Eq. (4-3) exhibits two distinct values of T_m at which $dT_m/d\tau$ is identically zero. Since our results show that both $\dot{m}_o$ and $\dot{q}$ are monotonically increasing functions of metal temperature T_m (see Figs. 4-2 and 4-3) only one solution for T_m is possible. This solution corresponds to the high temperature asymptotes displayed in Fig. 4-6. A formulation of the problem that allows for thermal diffusion and diffusional conduction within the steam/hydrogen film may reveal two metal temperatures for which $dT_m/d\tau$ is rendered zero. This generalization of the steam-film boundary layer problem is clearly beyond the scope of the present report.

Our results for the time for complete oxidation as a function of the strength of an incoming trigger shock is shown in Fig. 4-7. As previously mentioned, Lemmon [3] performed experiments in which very violent aluminum/water explosions were initiated with intense shocks produced with high-explosive charges. His measurements of pressure and light emitted from the reaction zone indicated that the very violent chemical reaction began approximately 1.0 millisecond after the shock reached the coarse premixture of water and aluminum. Figure 4-7 suggests that in order to oxidize a representative aluminum particle on this time scale a trigger shock of strength P_∞ = 7 MPa (~ 70 atm) is required. This is a rather intense steam explosion initiator. Indeed Lemmon found that only very high-intensity shocks produced damaging chemical explosions. Low or medium-intensity shocks were not very effective in this regard. Unfortunately, the actual initiator shock amplitudes were not reported by Lemmon so that a quantitative comparison between Fig. 4-7 and the measurements is not possible.

The apparent oxidation times, shown in Fig. 4-7, are based on the assumption that the aluminum particle is stationary while the surrounding liquid flows at the shock-induced velocity V_∞. Actually the particle accelerates from an initial low velocity (assumed to be negligibly small) to

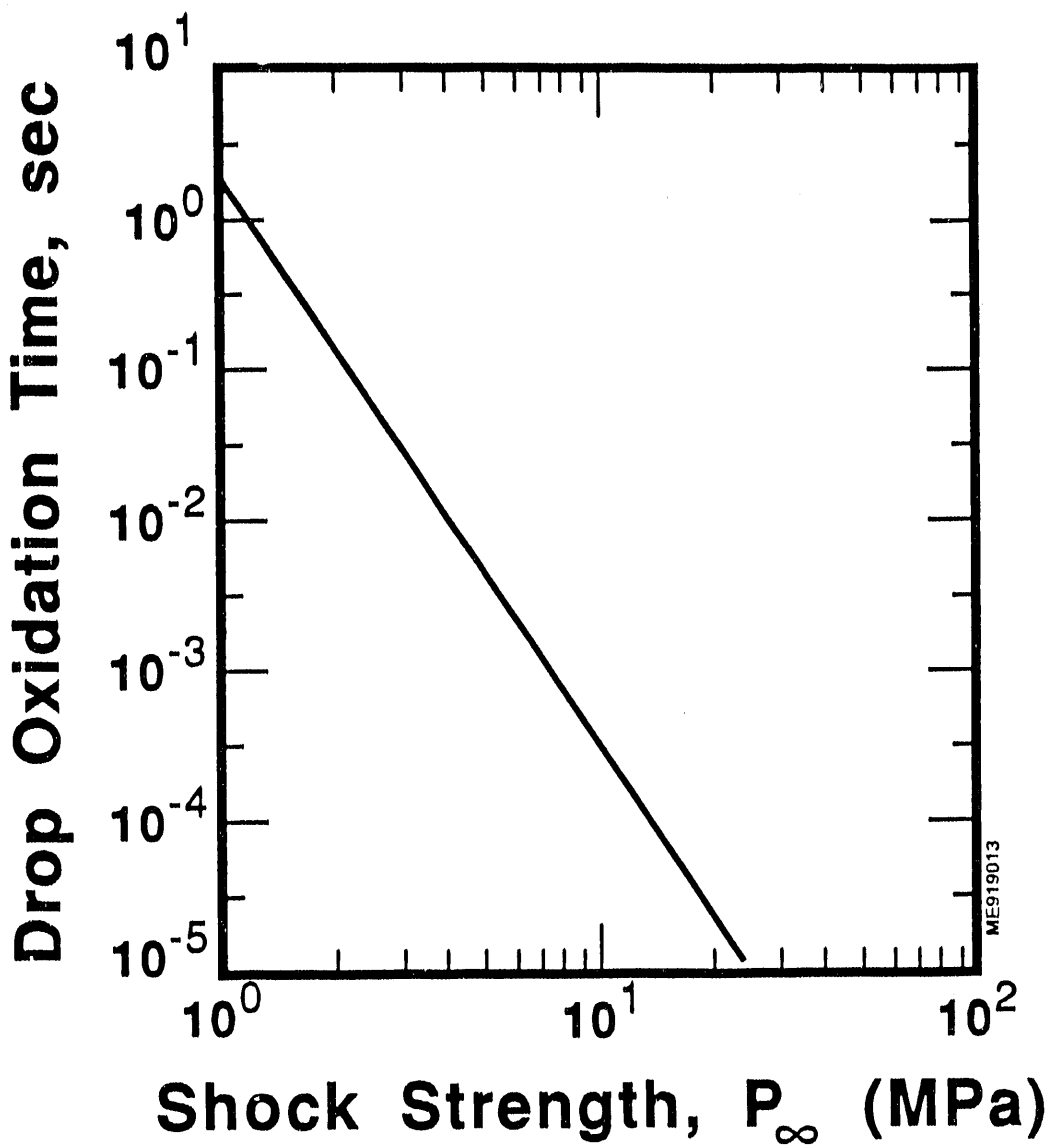

Figure 4-7 Aluminum particle (steam-transport controlled) oxidation time as a function of trigger shock pressure. Conditions; water instantaneously heated to saturation temperature corresponding to shock pressure, $T_m(o)$ = 1100K, γ = 0.5, e = 1.0.

the liquid velocity V_∞. From simple Newton's law considerations, the time τ_a it takes for a particle to accelerate up to some fraction F_u of the liquid velocity is given by the equation

$$\tau_a = \frac{8R\ \rho_m\ Re^m}{3N\ \rho_\ell\ V_\infty} \cdot \frac{(1 - F_u)^{-(1-m)} - 1}{(1 - m)} \qquad (4\text{-}7)$$

The above equation is based on the particle drag coefficient formula

$$C_D = \frac{N}{Re_u^m}$$

where Re_u is the particle "instantaneous Reynolds number" relative to the liquid and m and N are constants that depend on the particle flow regime. For $200 \leq Re_u \leq 10^3$; N = 3.6 and m = 0.313. For $10^3 < Re_u$; N = 0.44, m = 0. If the liquid kinematic viscosity is taken as $\nu_\ell = 2.9 \times 10^{-7}\ m^2\ s^{-1}$, then the time for a particle of radius R = 22.4 μm, produced in the wake of a 10 MPa shock (see Table 4-1), to accelerate to within 80 percent of the liquid velocity is τ_a = 0.15 msec (using N = 3.6 and m = 0.313). From the results of Fig. 4-7 and Table 4-1, the oxidation time for this particle is 0.32 msec. Thus the oxidation time should be corrected for variable V_∞. This can readily be accomplished with the present formalism which treats the transient heat and mass transfer external to the sphere as a succession of steady states. Without performing the analysis it is clear that taking particle acceleration into account would increase the oxidation time for a given shock pressure. An equivalent statement is that even larger predicted initiator shock pressures than those indicated by the curve in Fig. 4-7 would be required in order for chemical energy to contribute to the subsequent explosion.

It is apparent from the foregoing discussion that conditions must be "ripe" for a strong aluminum/water physical steam explosion before rapid chemical reaction provides the large energy release for a damaging explosion. A necessary condition for such an explosion is the presence of a shock that is strong enough to fragment the coarse metallic drops in the

aluminum/water premixture into millions of much smaller drops. If such a shock is transmitted into the coarse mixture, the steam transport-controlled oxidation rate is capable of keeping up with the fluid-mechanical and heat transport processes that drive the explosion. It is important to emphasize once again that the natural production of a shock strong enough to "ignite" the aluminum appears to be a rate event. Almost all the reported explosive events involving aluminum/water mixtures in inert smooth-walled containers required an artificially produced shock. The only reported naturally initiated explosion occurred in the first test of the test series carried out by Rightly and Beck [4], although no convincing arguments were presented by the authors that the premature firing of the trigger device in this test did not initiate the explosion (see Introduction). Perhaps the rather quiescent film boiling regime, in which the aluminum is separated from the water by a stable vapor layer in the premixing configuration, is not conducive to naturally occurring strong shocks and subsequent violent explosions.

5.0 CONCLUDING REMARKS

Encouraged by the success of the Turkdogan et al. [14] criterion for the limiting ambient oxygen concentration below which a metal oxidation reaction may take place in the vapor phase rather than on the surface, we have extended the criterion to predict the minimum (critical) aluminum metal temperature for rapid vapor phase burning in gaseous environments and under water. The lowest metal temperature consistent with vapor phase burning is defined by the condition that the diffusive/convective supply of steam can be accommodated by the maximum possible rate of metal evaporation, namely vaporization into a vacuum. This criterion, when combined with a standard film theory mass-transfer model, suggests that the observed ignitions of aluminum in gaseous environments is a transition to a vapor phase burning process. Estimates of the critical temperature for underwater vapor phase burning of a reactive aluminum sphere were made by using an available steam-hydrogen counter flux film-boiling model (Epstein et al.) and equating the steam flux to the sphere with the stoichiometrically equivalent maximum metal supply rate.

Vapor phase burning is predicted to be possible for pure aluminum and aluminum alloy spheres in free-fall through water providing that the initial aluminum melt temperature exceeds about 1950K for pure aluminum and about 1300K for 6063 aluminum alloy. The latter prediction is based on the vapor phase burning of the trace magnesium component of 6063 aluminum. These predictions are in good qualitative agreement with measured values of the aluminum-melt threshold temperatures for ignition-type steam explosions; however, they overestimate the measured threshold temperatures by about 150K. Interestingly enough, the model leads to the conclusion that vapor phase burning is not very likely to occur during the course of a steam explosion. Thus if we choose to interpret chemical ignition in terms of vapor phase burning we are led to speculate that the ignition process may be started by vapor phase burning in the aluminum-water premixture configuration but continues by rapid surface burning as the steam explosion evolves.

There is obviously a need to refine the critical temperature estimates for underwater vapor phase burning and, perhaps, to seek an alternative, more plausible ignition mechanism. It is recommended that attention be given the following physiochemical phenomena, mentioned previously but not yet pursued:

1. Thermal diffusion and diffusional conduction in the steam/hydrogen film, and their role in the overall reactive aluminum sphere energy balance that determines sphere heatup or quench.

2. Small-time transient steam-film heat- and mass-transport effects that may influence the predicted critical temperature for vapor phase burning before and during the explosion event.

3. The thermal and/or mechanical stability of the protective oxide film in determining the conditions for rapid surface reactions.

4. The oxidation rates of aluminum in steam at moderately high temperatures (~ 1100 - 1500K) and at pressure levels typical of steam explosion events.

5. The role of volatile additions to aluminum (e.g., magnesium) in determining the threshold temperature for chemical involvement in large-scale (~ 10 kg) steam explosions.

The first three items should be tackled analytically while Items 4 and 5 require experimental work.

6.0 NOMENCLATURE

a	Stagnation point velocity gradient for the H_2O-H_2 film, Eq. (3-4).
a_ℓ	Stagnation point velocity gradient for the liquid, Eq. (3-4).
A	Dimensionless metal surface superheat parameter, Eq. (3-18).
B	Dimensionless liquid (water) subcooling parameter, Eq. (3-18).
c	Heat capacity.
c_s	Sound speed in water.
C_D	Metal sphere drag coefficient.
D	Fick's molecular diffusion coefficient for the product gas-oxidizer gas species.
e	Total emittance of the reactive surface, Eq. (3-1).
f	Dimensionless H_2O-H_2 film flow stream function, Eq. (3-3).
F	Dimensionless liquid flow stream function, Eq. (3-2).
F_m	Fraction of reacted molten metal sphere.
F_u	Ratio of particle velocity to liquid velocity, Eq. (4-7).
Gr	Grashof number, Eq. (2-20).
h_{fg}	Latent heat of liquid (water).
ΔH	Heat release per mole of metal reacted, Eq. (3-38).
I	Inert product gas species.
k	Thermal conductivity.
L	Characteristic dimension of reacting metal body.
$\dot{m}_o, \dot{m}_I$	Oxidation and product gas mass flux.
$\dot{m}_{o,low}$	Oxidizer gas mass flux at low-mass-flux conditions.
$\dot{m}_{vac}$	Metal vaporization rate into a vacuum.
$\dot{m}$	Total mass flux in product gas + oxidizer gas, Eq. (2-9).

M	Molecular weight.
Me	Metal species.
n	Moles of oxidizer gas removed per mole of metal reacted, Eq. (2-2).
Ox	Oxidizer gas species.
P_{eq}	Saturation pressure of the vapor at the vapor-liquid interface, Eq. (3-19).
$P_{eq,m}$	Equilibrium vapor pressure of metal.
P	Pressure.
P_a	Pressure in ambient medium in front of "trigger shock".
Pr	Prandtl number, ν/α.
$\dot{q}$	Convective heat flux at the reacting surface, Eq. (3-20).
$\dot{q}_{rad}$	Radiation heat flux at the reacting surface, Eq. (3-1).
Q_{rad}	Dimensionless radiation heat flux, Eq. (3-17).
r	Radial (or arc length) measured from the stagnation point, Fig. 3-1.
R	Radius of reacting metal sphere.
$\bar{R}$	Universal gas constant.
Re	Reynolds number of reacting metal sphere, $2RV_\infty/\nu_\ell$.
s	Moles of inert gas produced per mole of metal vapor reacted, Eq. (2-2).
Sc	Schmidt number, ν/D.
Sh	Sherwood number, Eq. (2-14).
t,T	H_2O-H_2 film and liquid (water) temperatures, respectively.
T_m	Temperature of reacting metal sphere.
$T_{m,cr}$	Critical (minimum) metal temperature for vapor phase burning.
ΔT	Temperature difference between metal and ambient gas.
T_r	Reference temperature for physical property evaluation.

u,U	H_2O-H_2 film and liquid velocities in the r-direction, respectively, Fig. 3-1.
v,V	H_2O-H_2 film and liquid velocities in the z-direction, respectively, Fig. 3-1.
y	Coordinate normal to reaction front (or metal surface) in film model of boundary layer, Fig. 2-1.
Y	Mass fraction of oxidizer gas.
Y_r	Reference mass fraction for physical property evaluation.
z	Coordinate normal to the reacting surface in film-boiling stagnation flow model, Fig. 3-1.

Greek Symbols

α	Thermal diffusivity.
β	$(\nu\rho^{1/2})^{1/2}$ ratio, Eq. (3-17).
β_T	Coefficient of thermal expansion.
γ	"Weighting" factor for physical property evaluation in H_2O-H_2 film, Eq. (3-22).
δ	Boundary layer thickness (Fig. 2-1) or H_2O-H_2 film thickness, Fig. 3-1.
ϵ	Density ratio, Eq. (3-17).
η	Dimensionless similarity coordinate for H_2O-H_2 film, Eq. (3-3).
η_δ	Dimensionless H_2O-H_2 film thickness, $\delta(2\alpha/\nu)^{1/2}$.
θ	Dimensionless H_2O-H_2 film temperature, Eq. (3-5).
μ	Absolute viscosity.
ν	Kinematic viscosity (μ/ρ).
ξ	Dimensionless similarity coordinate for the liquid, Eq. (3-2).
ρ	Density.
σ	Stefan-Boltzmann radiation constant, Eq. (3-1).
σ_ℓ	Surface tension of liquid (water).
σ_m	Surface tension of molten metal.

τ Time.

τ_a Metal particle (sphere) acceleration time, Eq. (4-7).

ϕ Dimensionless liquid temperature, Eq. (3-5).

ω Dimensionless mass fraction of steam, Eq. (3-5).

Subscripts*

i At boiling liquid interface, Fig. 3-1.

I Inert product gas.

ℓ Liquid properties.

m Reacting metal (aluminum).

mix Pertains to gas mixture.

o Oxidizer gas.

∞ Conditions in the liquid or ambient gas far from the reaction front or surface.

---

*. Unsubscripted physical properties α, μ, ρ, k, ν, and D in the film-boiling stagnation flow model pertain to the H_2O-H_2 film.

7.0 REFERENCES

1. G. Long, "Explosions of Molten Aluminum in Water - Cause and Prevention", Metal Progress, 71, 107-112 (1957).

2. P. D. Hess and K, J. Brondyke, "Causes of Molten Aluminum-Water Explosions and Their Prevention", Metal Progress, 95, 93-100 (1969).

3. A. W. Lemmon, Jr., "Explosions of Molten Aluminum and Water", Light Metals, Metallurgical Society of AIME, Warrendale, PA, 817-836 (1980).

4. M. J. Rightly and D. F. Beck, "NPR/FCI EXO-FITS Experiment Series Report", Limited Distribution Draft for Review, SAND91-1544, Sandia National Laboratories (June, 1991).

5. L. S. Nelson, P. M. Duda, and D. A. Hyndman, "Thermal- and Ignition-Type Steam Explosions", Presented at AERO FCI Meeting, Orlando, FL (June 4, 1991).

6. P. Kuan and B. J. Buescher, "Ignition Threshold of Molten Aluminum in Water", AIChE Symposium Series, 87, 177-181 (1991).

7. H. M. Higgins and R. D. Schultz, "Reaction of Metals with Water and Oxidizing Gases at High Temperatures", Aerojet General Corporation, IDO-28000 (1957).

8. M. J. Young and L. S. Nelson, "Oxidation of Molten Fuel Simulant Drops Under Film Boiling Conditions", Presented at ANS International Topical Meeting on Safety of Thermal Reactors, Portland, OR (July 22-25, 1991).

9. M. Epstein, J. C. Leung, G. M. Hauser, R. E. Henry, and L. Baker, Jr., "Film Boiling on a Reactive Surface", Int. J. Heat Mass Transfer, 27, 1365-1378 (1984).

10. L. T. Pong, "A Theoretical Study of the Reactions of Molten Zr, Fe, and Al with Water", Sandia National Laboratories, SAND88-7119 (1988).

11. L. Baker, Jr. and R. Simms, "Status of Technology of Oxidation and Hydrogen Generation", Draft Report, ANL/NPR-90/024, Argonne National Laboratory (September, 1990).

12. D. K. Kuehl, "Ignition and Combustion of Aluminum and Beryllium", AIAA Journal, 3, 2239-2247 (1965).

13. J. Glassman, "Combustion of Metals. Physical Considerations", in Solid Propellant Rocket Research, Academic Press, New York, 253-258 (1967).

14. E. T. Turkdogan, P. Grieveson, and L. S. Darken, "Enhancement of Diffusion-Limited Rates of Vaporization of Metals", J. Physical Chemistry, 67, 1647-1654 (1963).

15. P. B. Spalding, Convective Mass Transfer, McGraw-Hill, New York (1963).

16. S. Nakai and T. Okazaki, in Buoyancy-Induced Flows and Transport, B. Gebhart et al., Hemisphere, New York, 207 (1988).

17. T. E. Daubert and R. P. Danner, "Data Compilation Tables of Properties of Pure Compounds", Design Institute for Physical Property Data, AIChE, 345 East 47th Street, New York, NY 10017.

18. E. M. Sparrow and J. L. Gregg, "Free Convection with Variable Properties", J. Heat Transfer, 80, 879-895 (1958).

19. O. Kubaschewski, E. W. Evans, and C. B. Alcock, Metallurgical Thermochemistry, 4th ed., Pergamon Press, Oxford (1967).

20. G. P. Raithby and K. G. T. Hollands, in Buoyancy-Induced Flows and Transport, B. Gebhart et al., Hemisphere, New York, 213 (1988).

21. E. R. G. Eckert and R. M. Drake, Jr., Analysis of Heat and Mass Transfer, McGraw-Hill, New York (1972).

22. R. E. Wilson, C. Barnes, and L. Baker, Jr., "Studies of the Aluminum-Steam Reaction by the Levitation Melting Method", Chemical Engineering Division Semiannual Report, January-June, 1964, USAEC Report ANL-6900, 233, Argonne National Laboratory (1964).

23. A. G. Merzhanov, Y. M. Grigorjov, and Y. A. Galchenko, "Aluminum Ignition", Combustion and Flame, 29, 1-14 (1977).

24. M. Epstein and G. M. Hauser, "Subcooled Forced-Convection Film Boiling in the Forward Stagnation Region of a Sphere or Cylinder", Int. J. Heat Mass Transfer, 23, 179-189 (1980).

25. R. C. Crooks, P. G. Hershall, H. A. Sorgenti, A. W. Lemmon, Jr., and R. B. Filbert, Jr., "Studies Relating to the Reaction Between Zirconium and Water at High Temperatures", (Edited by A. W. Lemmon, Jr.), Report BMI-1154, Battelle Memorial Institute, Columbus, OH (May, 1962).

26. L. Baker, Jr. and L. C. Just, "Studies of Metal-Water Reactions at High Temperatures III - Experimental and Theoretical Studies of the Zirconium-Water Reaction", Report ANL-6548, Argonne National Laboratory, Argonne, Illinois (May, 1962).

27. H. Schlichting, Boundary Layer Theory, 4th ed., McGraw-Hill, New York (1960).

28. R. C. Reid and T. K. Sherwood, The Properties of Gases and Liquids, Their Estimation and Correlation, 2nd ed., McGraw-Hill, New York (1966).

29. C. W. Gear, Numerical Initial Value Problems in Ordinary Differential Equations, Prentice Hall, Englewood Cliffs, NJ (1971).

30. A. C. Hindmarsh, "Linear Multistep Methods for Ordinary Differential Equations: Method Formulations, Stability, and the Methods of Nordsieck and Gear", Lawrence Livermore National Laboratory Report UCRL-51185, Rev. 1 (March, 1972).

31. P. N. Rose, "Drag Forces in a Hydraulic Model of a Fluidized Bed - Part II", Trans. Inst. Chem. Engrs., 39, 175-180 (1961).

32. M. Epstein and H. K. Fauske, "Steam Film Instability and the Mixing of Core-Melt Jets and Water", Proc. ANS 1985 National Heat Transfer Conference, Denver, CO, 277-287 (August 4-7, 1985).

END

DATE
FILMED
5/18/92